STUDIES OF ELECTRIC FIELD ASSISTED SOLVENT DRYING FOR EFFICIENT BULK HETEROJUNCTION SOLAR CELLS

A Thesis

Submitted in partial fulfillment for the degree of

MASTER OF SCIENCE

(Material Science)

By

A.V. RAAGHESH

CHEMISTRY AND PHYSICS OF MATERIALS UNIT

JAWAHARLAL NEHRU CENTRE FOR ADVANCED SCIENTIFIC RESEARCH

(A DEEMED UNIVERSITY)

Bangalore – 560064

Dedicated to my parents

Declaration

I hereby declare that the matter embodied in the thesis entitled *"**STUDIES OF ELECTRIC FIELD ASSISTED SOLVENT DRYING FOR EFFICIENT BULK HETEROJUNCTION SOLAR CELLS"*** is the result of the work carried out by me under the supervision of Prof. K. S. Narayan, at Molecular Electronics Laboratory, in Chemistry and Physics of Materials Unit, Jawaharlal Nehru Centre for Advanced Scientific Research, Bangalore, India. It has not been submitted for the award of any degree or diploma or associateship of any other university or institute.

In keeping with the general practice in reporting scientific observations, due acknowledgement has been made whenever the work described is based on the findings of other investigators.

(A. V. Raaghesh)

JAWAHARLAL NEHRU CENTRE FOR ADVANCED SCIENTIFIC RESEARCH

Bangalore – 560064

K. S. NARAYAN
Professor
Dean (Research and Development)
Phone: +91 80 2208 2822/2548
E-mail: narayan@jncasr.ac.in
Fax: + 91 80 2208 2766

April 8th, 2014

Certificate

I hereby certify that the matter embodied in this thesis entitled *"**STUDIES OF ELECTRIC FIELD ASSISTED SOLVENT DRYING FOR EFFICIENT BULK HETROJUNCTION SOLAR CELLS**"* is the result of the work carried out by Mr. A.V. Raaghesh at the Molecular Electronics Laboratory, in Chemistry and Physics of Materials Unit, Jawaharlal Nehru Centre for Advanced Scientific Research, Bangalore, India, under my supervision and it has not been submitted for the award of any degree or diploma or associateship of any other university or institute.

Prof. K. S. Narayan

(Research supervisor)

Acknowledgements

I would like to express my sincere thanks to my research supervisor Prof. K. S. Narayan, for suggesting me this problem. His guidance and constant motivation have given me confidence in exploring the field.

I thank Prof. C.N.R. Rao for being a constant source of inspiration. The commitment Prof. Rao shows to science is contagious.

I am thankful to my present and past lab-mates, Dr. Anshuman, Dr. Kishore, Dr. Poonam, Dr. Murthy, Vini, Satyaprasad, Ravi, Prashant, Ashar, Swathi, Rishav, Vikas, Nishit, Madhu, Dhruv, Mathieu for their valuable discussions and their insights have helped me understand better. They have made working in lab interesting and worthwhile.

Dipa and Sonu for the wonderful times we had together. My close friends and batchmates Neelima, Pallabi, Debopreeti, Krishna, Mohini, Monali, Susheela, Komal, Abhijit, Rajib, Suchitra and Uttam for standing by me through my best and worst times. I thank my juniors-turned-friends Kushagra, Promit, Shantanu and Ananya. I thank my other friends and seniors at JNC, Dileep, Vasudevan, Tarak, Sankalp, Navaneeth, Gopal for helping me colour my life. I thank all my other friends, Integrated PhD family and well-wishers for making JNC a wonderful place for me.

Deepest gratitude is due to Prof. S. Balasubramaniam, Chairman of Chemistry and Physics of Materials Unit, for being the best person I know in JNC. I wish I could carry the advices you have given me all my life. I thank Dr. T.K. Maji for being encouraging and supportive. I thank my course instructors at JNC, Prof. Chandrabhas Narayana, Dr. Eswaramoorthy, Dr. Rajesh Ganapathy, Prof. S.M.Shivaprasad, Dr. A. Sundaresan, Dr. N.S.Vidhyadhiraja, Prof. Umesh Waghmare, Prof. G.U. Kulkarni, Prof. Shobhana Narasimhan, Dr. Ranjan Dutta, Prof. Aloknath Chakroborthy for their discussions and lectures.

My all-time best friends from kindergarden school days, Sajeev, Baiju, Vignesh and Manu. One of the factors moving my life ahead is the prospects of meeting you guys over again.

Gowtham, Susanth, Pradeep, Praba, Preethi, Varalakshmi and Sujithra for being friends with me, since BSc.

I owe alot to my teachers from school to graduation, especially Dr. C.K. Shashidharan Nair, Dr. Rajamani, Dr. Balakrishanan, Dr. Sabu and Dr. Shariff.

I also thank working staff at JNC and hostel for making life pleasant and easier.

My brother Rajish for being a good friend to me and for being the coolest person I know. Though you are younger to me, I have learnt and I am still learning a lot from you.

I have no words to thank my parents for the sacrifices they have made in their life, for getting me and my brother educated, for trusting me in every step, for standing by every decision I have made in my life. Dad, you will always live in our hearts.

Preface

Organic solar cells have attracted lot of attention as a cheap and viable option for sustained energy resource. However, several issues like energy efficiency, cost and stability have to be carefully addressed in realizing this. This thesis is an attempt to understand the role played by external fields in forming optimum film morphology to enhance power conversion efficiency.

In the first chapter we discuss the basic principles involved in the working of organic solar cells and recent strategies developed for controlling the film morphology to obtain optimum efficiency. In addition to the more popular ways of controlling morphology by varying blend ratio and annealing, thesis addresses the use of electric field induced control alignment of the constituent species.

Second chapter deals with the materials and methods involved in the fabrication of solar cells as well as the experimental techniques used to characterize the devices.

Third chapter shows enhancement in performance of a solar cell fabricated from a crystalline donor solar cell by the application of electric field during its drying stage. A 30% increase in performance is obtained by comparing with thermally annealed devices fabricated under similar conditions.

Fourth chapter demonstrates the effect of electric field induced morphology in an amorphous donor solar cell. Usage of electric field during thermal annealing is found to be detrimental for the devices while applying electric field during the vacuum drying of the samples enhances efficiency. This is attributed to favourable structural modifications induced by electric field.

Table of Contents

Chapter 1: General Introduction 1

1.1 Introduction to organic electronics 1

1.2 Organic solar cells (OSC) 2

1.2.1 Early advancements in organic solar cells (OSC) 2

1.2.2 Working principle of organic solar cells (OSC) 3

1.2.3 Quantum efficiency of organic solar cell 4

1.2.4 Device structures 5

1.3 Active layer film formation 5

1.3.1 Thermal annealing 6

1.3.2 Solvent annealing 6

1.3.3 Use of additives 6

1.4 Electric field induced alignment in systems 7

1.4.1 Application electric field on a molecule 7

1.4.2 Liquid crystals 8

1.4.3 Ferroelectric polymers 9

1.4.4 Electric field patterning of thin films 9

1.4.5 Previous electro-hydro-dynamic instability reports from our lab 10

1.4.6 Review of electric field poling in OSC 11

1.5 Scope of thesis 11

1.6 References 12

Chapter 2: Materials and methods 19

2.1 Materials 19

2.1.1 Donor molecules 19

2.1.1.1 P3HT 19

2.1.1.2 PBDTTT-C-T 21

2.1.2 Acceptor molecules 21

2.1.2.1 $PC_{60}BM$ 21

2.1.2.2 $PC_{70}BM$ 21

2.1.3 Buffer layers 22

2.1.3.1 Hole buffer layer 22

2.1.3.2 Electron Buffer layer 23

2.1.4 Additives 23

2.1.5 Electrodes 23

2.2 Processes involved in solar cell fabrication 24

2.2.1 Etching of ITO 24

2.2.2 RCA treatment 24

2.2.3 Thermal deposition 24

2.3 Characterization of an organic Solar cell 25

2.3.1 Current density – voltage measurement 25

2.3.2 IPCE measurement 27

2.3.3 Atomic force microscopy (AFM) 28

2.4 References 29

Chapter 3 : Electric field assisted solvent drying in P3HT: $PC_{60}BM$ solar cells 33

3.1 P3HT:$PC_{60}BM$ BHJ system 33

3.1.1 Device 33

3.1.2 P3HT:$PC_{60}BM$ solution preparation 33

3.1.3 ZnO sol preparation 34

3.1.4 ZnO NP preparation 34

3.2 Active layer 34

3.2.1 Fabrication of polymer thin film 34

3.2.2 Thermal annealing of active layer 35

3.2.3 Thermal annealing of active layer in electric field 35

3.3 Organic solar cell characterization 36

3.3.1 Solar cell based on zinc acetate buffer layer 36

3.3.1.1 J-V characterization 36

3.3.2 Solar cell based on ZnO nano dispersion buffer layer 37

3.3.2.1 J-V characterization: 38

3.3.2.2 IPCE 39

3.3.2.3 AFM results 39

3.4 Discussion 43

3.5 Conclusion and future directions 44

3.6 References 44

Chapter 4: Electric field assisted solvent drying in PBDTTT-C-T: $PC_{70}BM$ solar cells 47

4.1 PBDTTT-C-T: $PC_{70}BM$ BHJ blend system 47

4.2 Device fabrication 47

4.2.1 PBDTTT-C-T: $PC_{70}BM$ solution preparation 47

4.3 Thermal annealing and thermal annealing in electric field 48

4.3.1 J-V characteristics of UA, TA and TAIE samples 48

4.4 Vacuum treatment and electric field under vacuum 49

4.4.1 Experimental setup 50

4.4.2 J-V characteristics of UA, VT and VTIE samples 50

4.4.3 IPCE spectrum 51

4.5 Discussion 52

4.5.1 Latest batch 53

4.6 Conclusion and future directions 54

4.7 References 55

List of Figures

Figure 1. 1: Advancements in organic solar cells design 2
Figure 1. 2: Steps involved in the working of organic solar cells. The steps are labeled with numbers within white circles 3
Figure 1. 3: Device structures of solar cell 5
Figure 1. 4: Alignment of a molecule in electric field. Blue lines indicate the electric field lines. 7
Figure 1. 5: Alignment of liquid crystal under electric field. Blue lines indicate the Electric field lines. 8
Figure 1. 6: The image shows pillar formation in thin film (depicted in blue colour) placed between electrodes (depicted in grey) 10

Figure 2. 1: Donors and acceptors used 20
Figure 2. 2: Etching of ITO 24
Figure 2. 3: Current density - voltage characteristics of a solar cell 26
Figure 2. 4: Schematic diagram of J-V measurement setup 26
Figure 2. 5: Schematic diagram of IPCE measurement setup 27
Figure 2. 6: Schematic diagram of AFM arrangement for surface studies on the device 28

Figure 3. 1: The band levels of ITO/ZnO/P3HT: $PC_{60}BM/MoO_3$/Ag. The numerical values in the image are electron energy values in eV. 34
Figure 3.2: Schematic of experimental setup for thermal-annealing-in-electric-field of the samples 35
Figure 3. 3: J-V characteristics of best devices under different treatments for ITO/ZnO (Sol)/P3HT:$PC_{60}BM/MoO_3$/Ag samples 36
Figure 3. 4: J-V characteristics of best devices under different treatments for ITO/ZnO (NP)/P3HT:$PC_{60}BM/MoO_3$/Ag samples 38

Figure 3. 5: IPCE spectrum of ITO/ZnO (NP)/P3HT:$PC_{60}BM$/MoO_3/Ag under different treatments 39
Figure 3. 6: AFM phase image and topographic images of un-annealed (UA) samples 40
Figure 3. 7: AFM phase image and topographic images of thermally annealed (TA) samples 41
Figure 3. 8: AFM phase image and topographic images of thermally annealed samples in Electric field (TAIE) samples 42
Figure 3. 9: Schematic representation of the film morphology of P3HT: $PC_{60}BM$ OSCs when the samples are un-annealed (a), thermally annealed (b), thermally annealed in electric field (c).The red coloured strips indicate P3HT chains and blue circles indicate PCBM. 43

Figure 4. 1: The band levels of ITO/ZnO/PBDTTT-C-T: $PC_{70}BM$/MoO_3/Ag. The numerical values in the image are electron energy values in eV 48
Figure 4. 2: J-V characteristics for best device performance of ITO/ZnO (NP)/PBDTTT-C-T: $PC_{70}BM$/MoO_3/Ag for UA, TA and TAIE samples. 49
Figure 4. 3: J-V characteristics for best device performance of ITO/ZnO (NP)/PBDTTT-C-T: $PC_{70}BM$/MoO_3/Ag for UA, VT and VTIE samples 51
Figure 4. 4: IPCE spectrum of ITO/ZnO (NP)/PBDTTT-C-T: $PC_{70}BM$/MoO_3/Ag for UA, VT and VTIE samples 52
Figure 4. 5: Schematic representation of morphological changes induced when the samples are unannealed, vacuum treated (a); thermally annealed, thermally annealed in electric field (b); vacuum treatment in electric field (c) 52
Figure 4. 6: J-V characteristics of best device of ITO/ZnO (NP)/PBDTTT-C-T: $PC_{70}BM$/MoO_3/Ag (UA sample) 54

List of tables

Table 3. 1: Average and best of device performance of ITO/ZnO(Sol)/P3HT:$PC_{60}BM$/MoO_3/Ag under different treatments..... 36

Table 3. 2: Average and best of device performance of ITO/ZnO (NP)/P3HT:$PC_{60}BM$/MoO_3/Ag under different treatments 38

Table 4. 1: Average and best device performance of ITO/ZnO (NP)/PBDTTT-C-T: $PC_{70}BM$/MoO_3/Ag for UA, TA and TAIE samples..... 49

Table 4. 2: Average and best device performance of ITO/ZnO (NP)/PBDTTT-C-T: $PC_{70}BM$/MoO_3/Ag for UA, VT and VTIE samples..... 51

Table 4. 3: Average and best device performance of ITO/ZnO (NP)/PBDTTT-C-T: $PC_{70}BM$/MoO_3/Ag cells of the latest batch where ZnO thickness was varied (only UA samples) 53

Chapter 1

General Introduction

1.1 Introduction to organic electronics

Semiconducting properties have been discovered in certain classes of organic materials, with charge transport properties different than those in conventional inorganic materials like silicon. These classes of organic materials include long chain conjugated polymers. Polymer systems having alternating double bond along the backbone and have a finite overlap are commonly referred as conjugated polymers. Conductivity in these systems is due to the extended electron pathway due to the delocalized p_z electrons on the polymer backbone[1-3]. The resonant coupling between the p_z electrons causes the p_z orbitals to split into two energy states. The orbital with the lower energy state is the Bonding Molecular Orbital. It is also called Highest Occupied Molecular Orbital (HOMO) since it is completely filled. The higher energy state is the Anti-Bonding Molecular Orbital. This is unoccupied and is generally referred to as Lowest Unoccupied Molecular orbital (LUMO). In conjugated polymer systems, due to the wavefunction overlap of neighbouring unit cells, the HOMO and LUMO behave like bands analogous to the valence and conduction bands in inorganic semiconductors respectively. Thus the conjugated polymers can be equated to a semiconductor with a band gap. The optical bandgap of these conjugated polymers typically is in the range of 1.2 – 3.5 eV.

A major breakthrough occurred in the field during the year 1977[4], when it was discovered that doping of polyacetylene increased its conductivity from 10^{-5} Scm^{-1} to 10^{3} Scm^{-1}. The conductivity obtained on doping was almost comparable to the conductivity in metals (~10^{5} Scm^{-1} for copper). Since then doping induced increase in conductivity has been observed in a variety of polymer systems like polypyrroles[5], polythiopenes[6], poly(Isothlanaphthene)[7] and poly(alkylthiophenes)[8]. Advancements in this field have made it possible to solution process films of semiconducting polymers.

These semiconducting polymer systems also show interesting electroluminescence and photovoltaic properties[9-11]. Our understanding of these properties have enabled us to make Organic Light Emitting Diodes[12-13] (which have already entered the market) and Organic solar cells (with efficiencies[14-15] close to 10%).

1.2 Organic solar cells (OSC)

Conductivity, along with high absorption coefficient and the ability to tune the absorption properties by changing the structure have made organic materials find applications in solar cells[16-20]. In pristine polymer semiconductors, photoexcitation of pristine polymer semiconductors result primarily in formation of excitons (bound electron-hole pairs). The electron and hole remain bound because of the strong force of attraction between them, owing to the smaller dielectric constant (~ 3) of these systems. In a solar cell, the exciton is dissociated by internal electric field and they result in mobile charges, contributing to current. This is referred to as the exciton model and it provides a consistent framework to explain the optical and optoelectronic properties.

1.2.1 Early advancements in organic solar cells (OSC)

Earlier solar cell devices made up of organic materials had a single organic layer between two metals which acted as electrodes. The work function of the metal electrode was important in deciding the direction of charge transport. The device with a single organic layer showed very low efficiencies of the order of 10^{-3} to 10^{-1}.

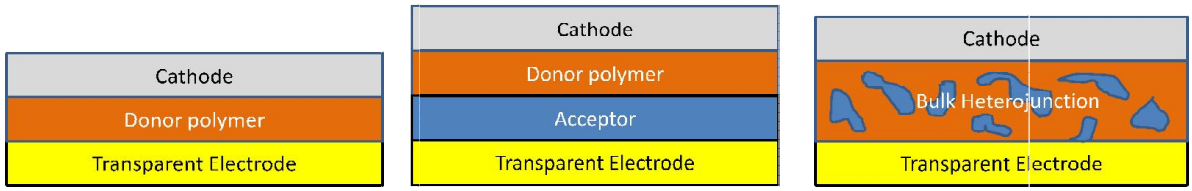

(a) Single layer SCs (b) Bilayer SCs (c) Bulk Heterojunction SCs

***Figure 1. 1**: Advancements in organic solar cells design*

The next generation of solar cell devices with two organic bilayers where one of the layers acted as donor and other layer acted as acceptor was fabricated. Internal electric field required to split the exciton is provided by the energy level offset of both the species. Their

performance was better than their predecessors. The limiting factor in bilayer solar cell was the exciton diffusion length (λ_d). λ_d is the distance an exciton travels in the polymer before recombination to ground state. In organic semiconductors (λ_d) is generally about 15 - 20nm[21]. This resulted in making layers of photoactive material thinner than λ_d, which then reduced number of photons absorbed.

Further improvement was obtained when the donor and acceptors were intermixed and spin-coated. This gave way to intermixed domains of acceptors and donors. The interpenetrated network of donors and acceptor species[22-24] enhanced efficiency considerably. This is referred to as Bulk-Heterojunction. The optimum domain size for Donor - Acceptor regions should be lesser or of the same length scale as the exciton diffusion length.

1.2.2 Working principle of organic solar cells (OSC)

The working of OSCs can be summarized by the following steps

1. Absorption of photon by donor species and creation of exciton
2. Diffusion of exciton to donor-acceptor interface
3. Exciton dissociation at the interface and formation of charge transfer state, which subsequently dissociates to form free charge carriers
4. Diffusion of separated charges to the respective electrodes

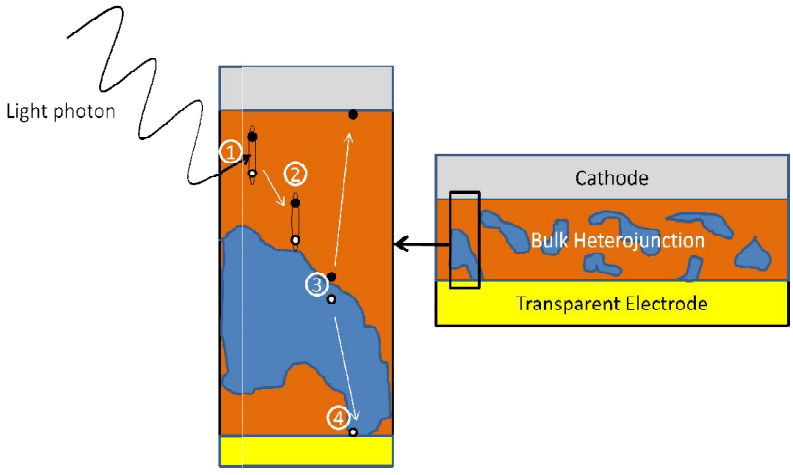

Figure 1. 2: *Steps involved in the working of organic solar cells. The steps are labeled with numbers within white circles*

1.2.3 Quantum efficiency of organic solar cell

Internal Quantum Efficiency (IQE) of an OSC is given by the product of the efficiency of each of four steps involved in the working of solar cells.

By definition, Internal Quantum Efficiency,

$$\eta_{IQE} = \eta_{AB}\eta_D\eta_{CT}\eta_{CC} \quad \text{.....(2)}$$

Here, η_{AB} is the efficiency of absorption of the incident light and it can be obtained from Beer Lambert's law. This can be increased by increasing the absorption of the system by tuning their structure to match the solar spectrum and by increasing the thickness of the film. η_D is the efficiency of the diffusion of formed exciton to the interface. η_D can be increased by having domain sizes smaller than the exciton diffusion length (λ_d). η_{CT} is the efficiency of the dissociation of exciton and formation of the charge-transfer state and its dissociation into free charges. It depends on morphology of the device and the choice of donor and acceptor. The charge transfer state can recombine without forming separated charges. This is called Geminate Recombination. η_{CC}, the efficiency of charge collection and depends on the interpenetrated network of the system and choice of electrode. The separated electron and holes can also recombine with opposite charge carriers on their path to respective electrodes. This is called Non-Geminate Recombination. The morphology of the film plays a critical role in deciding the efficiency of each of the above mentioned processes. Efforts have been taken to control film morphology to enhance efficiency and will be discussed more in the thesis.

External Quantum Efficiency (EQE) gives better picture of the efficiency of solar cell by considering external loss mechanisms. EQE is defined as the ratio of the number of electrons collected at the interface to the number of photons incident on the device.

$$\eta_{EQE}(\lambda) = \frac{n_{electrons-collected}}{n_{photons-absorbed}} = \frac{J*1240}{P*\lambda} \quad \text{.....(3)}$$

Here J_{sc} is the short circuit current density in A/cm^2, P is incident light power in W/cm^2. As seen from the definition, EQE is a function of incident wavelength (λ in nanometer).

1.2.4 Device structures

A typical solar cell has a thin layer of active material (BHJ blend) placed between two planar electrodes to collect holes and electrons. Most often electron and hole buffer layers are used between the active layer and electrodes to facilitate the transport of electrons and holes to their respective electrodes.

In normal structure, the transparent electrode acts as the hole collector and in inverted structure, transparent electrode acts as the electron collector. To facilitate electron collection, normal structure uses low work function metals which are prone to oxidation. This reduces the stability of the device. Inverted architecture overcomes the stability issues originating from the electrodes to some extent.

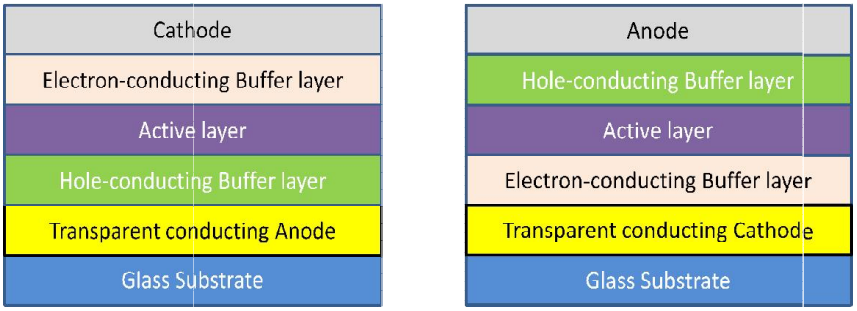

(a) normal device structure (b) inverted device structure

***Figure 1. 3**: Device structures of solar cell*

1.3 Active layer film formation

Spin-coating is the usual method employed by which active layer solution is cast into films. The morphology is decided by the phase separation of donor and acceptor regions. Optimum phase separation should lead to an interpenetrated network of donors and acceptors where the domain sizes are smaller than exciton diffusion length and the separated charge carriers should reach the electrodes without non-geminate recombination. This would lead to an enhancement in J_{sc} and FF of the device, without would inturn reflect in the power conversion efficiency.

Thus, understanding phase separation[25-27] and morphology evolution[28] of the active layer and controlling them is the need of the hour. Morphology of the device can be probed by X-ray

Scattering methods (Small and Wide Angle X-ray Scattering[29]; Polarized Xray Scattering[30]; Resonant Soft Xray Scattering[31]; Scanning Probe Microscopy[32-33] and Transmission Electron Microscopy[34].

The morphology of the film formed has been found to be depended on the components of the blend (donor, acceptor and solvent). For different donor-acceptor systems, different blend ratios are found to yield the optimum morphology. Choice of the solvent used also has been found to play a role in deciding the morphology film formed. Solvents with high boiling point which evaporate slowly have been found to help in the self-organization of the components in the film.

The following treatments are usually employed in improving the quality of the film, during or after the spin-coating of the blend.

1.3.1 Thermal annealing

Thermal annealing[35-36] is the process by which the spin-coated films are heated above their glass transition temperature for a short time. Thermal annealing helps in phase segregation of the polymer and acceptor molecules. It increases crystallization and domain sizes of the polymer. Thermal annealing also helps in making the films smoother and avoiding contact losses and trapping sites at the electrode. Over-annealing (annealing at very high temperatures or longer times) have been found to be detrimental to the device performance. Thermal annealing is efficient process only if the donor polymer is crystalline in nature.

1.3.2 Solvent annealing

Solvent annealing[37-38] is the process by which the spin-coated samples are placed in a solvent-vapour rich environment. This slows the rate of evaporation of the solvent from the film. Polymer films have been found to self-organize better when the rate of evaporation is slower, thereby reaching a better film morphology.

1.3.3 Use of additives

The additives[39-40] used are usually high boiling solvents which reduce the rate of evaporation even further. 1,8-di-iodo-octane(DIO)[38,39], alkyl-dithiols are some of the commonly used

additives. It is observed that the increase in efficiency of OPVs due to additives can be attributed to optimized phase segregation due to selective dissolution of acceptor molecule by the additive.

Electric field during drying of Thin Films

Another approach in contolling the film morphology is by using external fields like electric field. The effect of applying electric field during drying of active layer of the solar cell is the focus of this thesis and will be discussed in detail as we proceed through the thesis.

1.4 Electric field induced alignment in systems

1.4.1 Application electric field on a molecule

When external electric field is applied on a polar molecule, the molecule will experience a torque to align itself with the electric field thereby reducing the energy of the molecule. If the molecule does not have permanent dipole moment, it can form induced dipole moment, due to the displacement of centers of the positive and negative charge, under external electric field. The dipole moment in the case of polar molecule will be higher when compared with the dipole moment in a non-polar molecule.

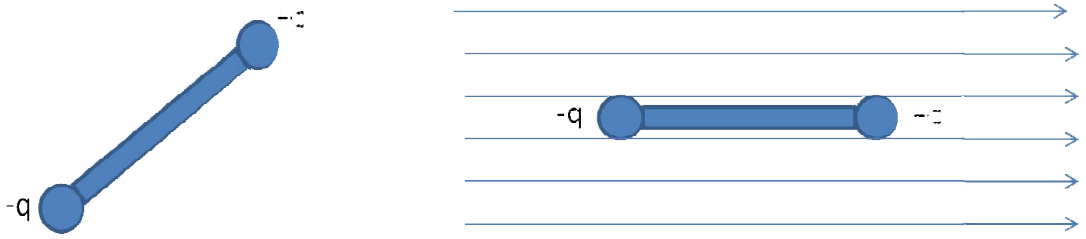

(a) No Electric field (b) Electric field applied

Figure 1. 4*: Alignment of a molecule in electric field. Blue lines indicate the electric field lines.*

The torque (τ) experienced by the molecule will depend on the dipole moment (p), the direction of the dipole moment and the external field applied (E).

$$\vec{\tau} = \vec{p} X \vec{E} \quad \text{.....(5)}$$

The potential energy (U) gained by the molecule on aligning is given by

$$U = \vec{p}.\vec{E} \quad \text{.....(6)}$$

Two important classes of organic materials worth discussing at this point are liquid crystals and Ferroelectric Polymers.

1.4.2 Liquid crystals

Liquid crystals are polymeric materials which have been found to exhibit properties like fluidity similar liquids and ordering of dipoles similar to ones present in solid crystals. They exhibit different phases as a function of temperature and concentration. These molecules have been found to align in external fields like electric and magnetic fields[41-42]. The field does not induce orientation order in the system, rather changes the direction of orientation of the molecules. Director (D), a vector of unit magnitude gives the direction of orientation of the molecules.

Free energy contribution (F_e) on aligning with the field external electric field E is given by,

$$F_e = -\frac{1}{2}\varepsilon_o \Delta\varepsilon (E.D)^2 \quad \text{.....(7)}$$

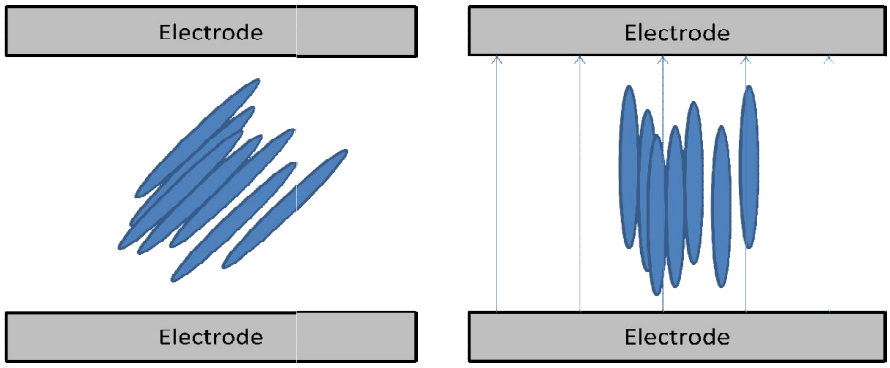

(a) No Electric field (b) Electric field applied

Figure 1. 5*: Alignment of liquid crystal under electric field. Blue lines indicate the Electric field lines.*

Here Δε is the difference in dielectric constant of the molecule along the direction of the director and perpendicular to it. Examples of liquid crystal polymers include Zenite 5145L,

kevlar and vectran. Alignment of liquid crystals in external electric field has been tapped in making displays where liquid crystals control the transmission of light through it.

1.4.3 Ferroelectric polymers

They are a class of crystalline polymers which have a strong inherent electric polarization in them[43-44]. They have a characteristic curie temperature above which phase transition to paraelectric region takes places. They exhibit characteristic hysteresis as in ferroelectric materials. Most of them possess piezoelectric and pyroelectric properties. Most studied polymer in this field is polyvinylidene fluoride (PVDF) and poly[(vinylidenefluoride-co-trifluoroethylene] [P(VDF-TrFE)] Ferroelectric polymers have found application in piezoelectric transducers, actuators and memory units.

1.4.4 Electric field patterning of thin films

Electric field induced pattern formation on soft films is termed Electro-Hydro-Dynamic Lithography. Polymer films are coated on one of the electrode and electric field is applied between the top and bottom electrode which are separated by an air gap. On application of electric field, enhancement in the amplitude of capillary waves present on the surface of the polymer is observed. The waves grow and reach the top electrode and form pillars with hexagonal symmetry and characteristic spacing. The characteristic spacing (λ) is given by

$$\lambda = 2\pi\left[\frac{\gamma U}{\varepsilon_o \varepsilon_p (\varepsilon_p - 1)^2}\right] E_p^{-3/2} \quad \text{.....(8)}$$

where U is the voltage applied, ε_o and is the dielectric constant of free space, ε_p is the relative permittivity of the medium, γ is the surface tension of polymer and E_p is the field strength in the medium. It was first observed by Steiner and Ulrich in Polystyrene[45]. Since then it has been observed in other thin films and polymer films. Polymer films are more suited for this, since if the pattering is done above its glass transition temperature, its structure could be retained as the films are cooled. If the top electrode is patterned (has projections) and when electric field applied on the thin layers, patterning of the thin film takes place to follow the master pattern of the top electrode.

Polymer bilayers can also be subjected to electric field to observe the above mentioned effects[46-48]. In these studies, it was seen that pillar formation takes place with the inner core of one of the polymer material and the outer core with the other polymer material. The difference between dielectric constant between the two films (dielectric contrast), thickness of the individual layers and viscoelastic properties of the films decide the role the individual layer plays and the pattern formed. Electric field has been used in the self-assembly of Block-co-polymers[49-52] to control the microdomain formation.

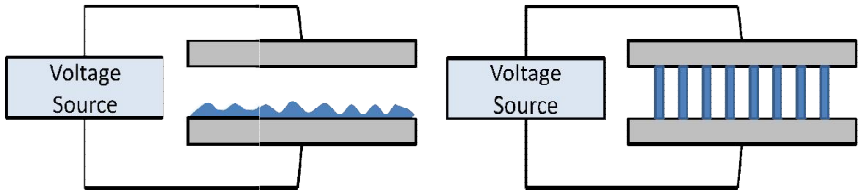

Figure 1. 6: *The image shows pillar formation in thin film (depicted in blue colour) placed between electrodes (depicted in grey)*

1.4.5 Previous electro-hydro-dynamic instability reports from our lab

Effect of electric field in the pattern formation of PDMS films between ITO and cover slip which acts as the other electrode was studied[53-54]. Edge straightening, finger elongation and pillar formation was found in different electric field regimes. It was also observed[55] that the soft thin films exhibited two visco-elastic regimes. Electric field induced wetting was used to move drops of polymer dispersion on micro-channels made of hydrophobic material[56]. In another study[57], a PDMS surface was electro-hydro-dynamically patterned to make arrays of microaxions. The pattern formed was found to create Bessel beams. Electric field was used to deform droplets of low-melting alloys by applying electric field whose shape can be retained in the droplets[58].

1.4.6 Review of electric field poling in OSC

Electric field has been used to control the morphology of the active layer. Detailed literature review is discussed as follows.

In 2003, Sariciftzi and their group applied electric bias during the post-thermal annealing of P3HT:PCBM devices[59]. They found an enhancement in current density to 8.5 mA cm^{-2}. Efficiency improved from 2.5% to 3.5% on thermal annealing in electric field.

Cindy X. Zhao et al[60]., in the year 2011, used AC electric field to align the P3HT: PCBM BHJ. The electric field was applied to a floating top electrode and ITO. The electric field was of the order of 10^5 V/cm and the frequency of operation was 10^{-3} Hz. The PCE of the devices increased from 2.89% to 3.14%. The same group reported[61], having optimized their AC electric field strength to $5.5–8.25*10^4$ V/cm. XRD data was used to understand the origin of the enhancement in efficiency and The intensity of the P3HT peak increased upon poling.

In 2012, Ching-Fuh Lin et al[62]., reported that efficiency of their P3HT: PCBM system increased from 3.16% to 3.51%, when electric field of $5.0*10^5$ V/m was externally applied to the device during its drying stage. The same group showed[63] that the increase in device efficiency was more when the external electric field was applied horizontally rather than when it was applied vertically.

S. Sundar Kumar Iyer and group studied effect of electric field on P3HT:PCBM BHJ solar cells[64]. The XRD studies showed increase in the intensity of P3HT peaks. From AFM studies, they saw an increase in the RMS roughness of the poled sample when compared with the unannealed sample. IPCE of these devices was also found to increase on poling. In their Photovoltaic Specialists Conference (PVSC), 2012 paper[65], they went further ahead and poling was done on P3HT hole-only device. In their bulk state, the increase in the SCLC mobility was studied upon poling. Zero field hole- mobility was found to increase on poling.

1.5 Scope of thesis

The photovoltaic performance of BHJ polymer solar cells are intimately correlated to the morphology and mircostructure of the films. Most of the studies on application of electric field to control the morphology have been tried on crystalline donor-BHJ systems. They have

attributed the increase in crystallinity of the donors as the reason for enhancement in the efficiency of the devices. We have experimentally tried to verify the field induced enhancement of efficiency in P3HT:$PC_{60}BM$ systems, where P3HT is a crystalline donor.

Thermal annealing has been found to be detrimental to device performance for low-band gap amorphous donor BHJ solar cells. We envisage that the electric field induced annealing can also control the morphology of such BHJ systems. Since the donor unit is further composed of donor-acceptor molecules, it is expected to have a high local dipole moment.

PBDTTT-C-T: $PC_{70}BM$ is chosen as a model system where PBDTTT-C-T is an amorphous donor. Electric field induced annealing in this system indicates enhanced performance. On the other hand, thermal annealing treatments were found to be detrimental to the device performance.

The systems we are detailing with are thin films of BHJ. In such a system, there would be interplay between many factors such as interaction between molecules (donor-donor, donor-acceptor, acceptor-acceptor), molecule-solvent interaction (donor-solvent, acceptor-solvent), the dielectric contrast between the different components of the blend (donors, acceptors, solvent), kinetics of solvent evaporation, viscoelastic properties of the blend. Using electric field, we want to overcome the factors restricting optimum film formation and promote interactions favouring interactions leading to the formation of optimum morphology.

If electric field induced annealing could be optimized, it could be considered as one of the post-treatment methods for controlling film morphology. We also propose that the treatment would be effective for both crystalline and amorphous donors-BHJ systems.

1.6 References

1 Bredas, J. L. & Street, G. B. Polarons, bipolarons, and solitons in conducting polymers. *Accounts of Chemical Research* **18**, 309-315, doi:10.1021/ar00118a005 (1985).

2 Coropceanu, V. *et al.* Charge Transport in Organic Semiconductors. *Chemical Reviews* **107**, 926-952, doi:10.1021/cr050140x (2007).

3 Heeger, A. J., Kivelson, S., Schrieffer, J. R. & Su, W. P. Solitons in conducting polymers. *Reviews of Modern Physics* **60**, 781-850 (1988).

4 Chiang, C. K. *et al.* Electrical Conductivity in Doped Polyacetylene. *Physical Review Letters* **39**, 1098-1101 (1977).

5 Gardini, G. P. in *Advances in Heterocyclic Chemistry* Vol. Volume 15 eds A. R. Katritzky & A. J. Boulton) 67-98 (Academic Press, 1973).

6 Hayes, W., Pratt, F. L., Wong, K. S., Kaneto, K. & Yoshino, K. Absorption of doped polythiophene in the middle and far infrared. *Journal of Physics C: Solid State Physics* **18**, L555 (1985).

7 Wudl, F., Kobayashi, M. & Heeger, A. J. Poly(isothianaphthene). *The Journal of Organic Chemistry* **49**, 3382-3384, doi:10.1021/jo00192a027 (1984).

8 Frommer, J. E. Conducting polymer solutions. *Accounts of Chemical Research* **19**, 2-9, doi:10.1021/ar00121a001 (1986).

9 Friend, R. H. *et al.* Electroluminescence in conjugated polymers. *Nature* **397**, 121-128 (1999).

10 Kearns, D. & Calvin, M. Photovoltaic Effect and Photoconductivity in Laminated Organic Systems. *The Journal of Chemical Physics* **29**, 950-951, doi:doi:http://dx.doi.org/10.1063/1.1744619 (1958).

11 Ghosh, A. K., Morel, D. L., Feng, T., Shaw, R. F. & Rowe, C. A. Photovoltaic and rectification properties of Al/Mg phthalocyanine/Ag Schottky-barrier cells. *Journal of Applied Physics* **45**, 230-236, doi:doi:http://dx.doi.org/10.1063/1.1662965 (1974).

12 Sekitani, T. *et al.* Stretchable active-matrix organic light-emitting diode display using printable elastic conductors. *Nat Mater* **8**, 494-499, doi:http://www.nature.com/nmat/journal/v8/n6/suppinfo/nmat2459_S1.html (2009).

13 Saxena, K., Jain, V. K. & Mehta, D. S. A review on the light extraction techniques in organic electroluminescent devices. *Optical Materials* **32**, 221-233, doi:http://dx.doi.org/10.1016/j.optmat.2009.07.014 (2009).

14 Scharber, M. C. & Sariciftci, N. S. Efficiency of bulk-heterojunction organic solar cells. *Progress in Polymer Science* **38**, 1929-1940, doi:http://dx.doi.org/10.1016/j.progpolymsci.2013.05.001 (2013).

15 Su, Y.-W., Lan, S.-C. & Wei, K.-H. Organic photovoltaics. *Materials Today* **15**, 554-562, doi:http://dx.doi.org/10.1016/S1369-7021(13)70013-0 (2012).

16 Nunzi, J.-M. Organic photovoltaic materials and devices. *Comptes Rendus Physique* **3**, 523-542, doi:http://dx.doi.org/10.1016/S1631-0705(02)01335-X (2002).

17 Li, G., Zhu, R. & Yang, Y. Polymer solar cells. *Nat Photon* **6**, 153-161 (2012).

18 Benanti, T. & Venkataraman, D. Organic Solar Cells: An Overview Focusing on Active Layer Morphology. *Photosynth Res* **87**, 73-81, doi:10.1007/s11120-005-6397-9 (2006).

19 Zhou, Y. *et al.* A Universal Method to Produce Low–Work Function Electrodes for Organic Electronics. *Science* **336**, 327-332, doi:10.1126/science.1218829 (2012).

20 Son, H. J., Carsten, B., Jung, I. H. & Yu, L. Overcoming efficiency challenges in organic solar cells: rational development of conjugated polymers. *Energy & Environmental Science* **5**, 8158-8170, doi:10.1039/c2ee21608f (2012).

21 Günes, S., Neugebauer, H. & Sariciftci, N. S. Conjugated Polymer-Based Organic Solar Cells. *Chemical Reviews* **107**, 1324-1338, doi:10.1021/cr050149z (2007).

22 Brédas, J.-L., Norton, J. E., Cornil, J. & Coropceanu, V. Molecular Understanding of Organic Solar Cells: The Challenges. *Accounts of Chemical Research* **42**, 1691-1699, doi:10.1021/ar900099h (2009).

23 Alam, M. A., Ray, B., Khan, M. R. & Dongaonkar, S. The essence and efficiency limits of bulk-heterostructure organic solar cells: A polymer-to-panel perspective. *Journal of Materials Research* **28**, 541-557, doi:doi:10.1557/jmr.2012.425 (2013).

24 Yu, G. & Heeger, A. J. Charge separation and photovoltaic conversion in polymer composites with internal donor/acceptor heterojunctions. *Journal of Applied Physics* **78**, 4510-4515, doi:doi:http://dx.doi.org/10.1063/1.359792 (1995).

25 Xu, Z. *et al.* Vertical Phase Separation in Poly(3-hexylthiophene): Fullerene Derivative Blends and its Advantage for Inverted Structure Solar Cells. *Advanced Functional Materials* **19**, 1227-1234, doi:10.1002/adfm.200801286 (2009).

26 Clark, M. D., Jespersen, M. L., Patel, R. J. & Leever, B. J. Predicting Vertical Phase Segregation in Polymer-Fullerene Bulk Heterojunction Solar Cells by Free Energy Analysis. *ACS Applied Materials & Interfaces* **5**, 4799-4807, doi:10.1021/am4003777 (2013).

27 Chen, F.-C., Lin, Y.-K. & Ko, C.-J. Submicron-scale manipulation of phase separation in organic solar cells. *Applied Physics Letters* **92**, -, doi:doi:http://dx.doi.org/10.1063/1.2835047 (2008).

28 Campoy-Quiles, M. *et al.* Morphology evolution via self-organization and lateral and vertical diffusion in polymer:fullerene solar cell blends. *Nat Mater* **7**, 158-164, doi:http://www.nature.com/nmat/journal/v7/n2/suppinfo/nmat2102_S1.html (2008).

29 Chiu, M.-Y., Jeng, U. S., Su, C.-H., Liang, K. S. & Wei, K.-H. Simultaneous Use of Small- and Wide-Angle X-ray Techniques to Analyze Nanometerscale Phase Separation in Polymer Heterojunction Solar Cells. *Advanced Materials* **20**, 2573-2578, doi:10.1002/adma.200703097 (2008).

30 Collins, B. A. *et al.* Polarized X-ray scattering reveals non-crystalline orientational ordering in organic films. *Nat Mater* **11**, 536-543, doi:http://www.nature.com/nmat/journal/v11/n6/abs/nmat3310.html#supplementary-information (2012).

31 Swaraj, S. *et al.* Nanomorphology of Bulk Heterojunction Photovoltaic Thin Films Probed with Resonant Soft X-ray Scattering. *Nano Letters* **10**, 2863-2869, doi:10.1021/nl1009266 (2010).

32 Douhéret, O. *et al.* Nanoscale electrical characterization of organic photovoltaic blends by conductive atomic force microscopy. *Applied Physics Letters* **89**, -, doi:doi:http://dx.doi.org/10.1063/1.2227846 (2006).

33 Palermo, V. *et al.* A Kelvin Probe Force Microscopy Study of the Photogeneration of Surface Charges in All-Thiophene Photovoltaic Blends. *Advanced Functional Materials* **17**, 472-478, doi:10.1002/adfm.200600122 (2007).

34 Love, J. A. *et al.* Film Morphology of High Efficiency Solution-Processed Small-Molecule Solar Cells. *Advanced Functional Materials* **23**, 5019-5026, doi:10.1002/adfm.201300099 (2013).

35 Kim, Y. *et al.* Device annealing effect in organic solar cells with blends of regioregular poly(3-hexylthiophene) and soluble fullerene. *Applied Physics Letters* **86**, 063502-063502-063503, doi:10.1063/1.1861123 (2005).

36 Li, G. *et al.* High-efficiency solution processable polymer photovoltaic cells by self-organization of polymer blends. *Nat Mater* **4**, 864-868 (2005).

37 Li, G. *et al.* "Solvent Annealing" Effect in Polymer Solar Cells Based on Poly(3-hexylthiophene) and Methanofullerenes. *Advanced Functional Materials* **17**, 1636-1644, doi:10.1002/adfm.200600624 (2007).

38 Li, G., Shrotriya, V., Yao, Y., Huang, J. & Yang, Y. Manipulating regioregular poly(3-hexylthiophene) : [6,6]-phenyl-C61-butyric acid methyl ester blends-route towards high efficiency polymer solar cells. *Journal of Materials Chemistry* **17**, 3126-3140, doi:10.1039/b703075b (2007).

39 Lee, J. K. *et al.* Processing Additives for Improved Efficiency from Bulk Heterojunction Solar Cells. *Journal of the American Chemical Society* **130**, 3619-3623, doi:10.1021/ja710079w (2008).

40 Lou, S. J. *et al.* Effects of Additives on the Morphology of Solution Phase Aggregates Formed by Active Layer Components of High-Efficiency Organic Solar Cells. *Journal of the American Chemical Society* **133**, 20661-20663, doi:10.1021/ja2085564 (2011).

41 Onuki, A. Liquid Crystals in Electric Field. *Journal of the Physical Society of Japan* **73**, 511-514, doi:10.1143/jpsj.73.511 (2004).

42 Williams, R. Liquid Crystals in an Electric Field. *Nature* **199**, 273-274 (1963).

43 Lim, S. H., Rastogi, A. C. & Desu, S. B. Electrical properties of metal-ferroelectric-insulator-semiconductor structures based on ferroelectric polyvinylidene fluoride copolymer film gate for nonvolatile random access memory application. *Journal of Applied Physics* **96**, 5673-5682, doi:doi:http://dx.doi.org/10.1063/1.1785836 (2004).

44 Hu, Z., Tian, M., Nysten, B. & Jonas, A. M. Regular arrays of highly ordered ferroelectric polymer nanostructures for non-volatile low-voltage memories. *Nat Mater* **8**, 62-67 (2009).

45 Schaffer, E., Thurn-Albrecht, T., Russell, T. P. & Steiner, U. Electrically induced structure formation and pattern transfer. *Nature* **403**, 874-877 (2000).

46 Leach, K. A., Gupta, S., Dickey, M. D., Willson, C. G. & Russell, T. P. Electric field and dewetting induced hierarchical structure formation in polymer/polymer/air trilayers. *Chaos: An Interdisciplinary Journal of Nonlinear Science* **15**, -, doi:doi:http://dx.doi.org/10.1063/1.2132248 (2005).

47 Lin, Z., Kerle, T., Russell, T. P., Schäffer, E. & Steiner, U. Structure Formation at the Interface of Liquid/Liquid Bilayer in Electric Field. *Macromolecules* **35**, 3971-3976, doi:10.1021/ma0122425 (2002).

48 Lin, Z., Kerle, T., Russell, T. P., Schäffer, E. & Steiner, U. Electric Field Induced Dewetting at Polymer/Polymer Interfaces. *Macromolecules* **35**, 6255-6262, doi:10.1021/ma020311p (2002).

49 Goldberg-Oppenheimer, P. *et al.* Hierarchical Orientation of Crystallinity by Block-Copolymer Patterning and Alignment in an Electric Field. *Chemistry of Materials* **25**, 1063-1070, doi:10.1021/cm3038075 (2013).

50 Li, G., Shi, L., Ye, Q., Zhou, W. & Tian, J. Electric-field-assisted assembly and alignment of polystyrene-b-poly(acrylic acid) micelles. *Colloid Polym Sci* **284**, 1179-1183, doi:10.1007/s00396-006-1495-6 (2006).

51 Liedel, C. *et al.* Electric-Field-Induced Alignment of Block Copolymer/Nanoparticle Blends. *Small* **9**, 3276-3281, doi:10.1002/smll.201202380 (2013).

52 Xu, T., Zhu, Y., Gido, S. P. & Russell, T. P. Electric Field Alignment of Symmetric Diblock Copolymer Thin Films. *Macromolecules* **37**, 2625-2629, doi:10.1021/ma035805g (2004).

53 Arun, N., Sharma, A., Shenoy, V. B. & Narayan, K. S. Electric-Field-Controlled Surface Instabilities in Soft Elastic Films. *Advanced Materials* **18**, 660-663, doi:10.1002/adma.200502199 (2006).

54 Arun, N., Sarkar, J., Sharma, A., Shenoy, V. B. & Narayan, K. S. Electric-Field Induced Morphological Transitions in Elastic Contact Instability of Soft Solid Films. *The Journal of Adhesion* **83**, 513-534, doi:10.1080/00218460701453486 (2007).

55 Arun, N. *et al.* Electric-Field-Induced Patterns in Soft Viscoelastic Films: From Long Waves of Viscous Liquids to Short Waves of Elastic Solids. *Physical Review Letters* **102**, 254502 (2009).

56 Narayan, K. S. & Rao, M. Electric-field-induced steering of conducting polymer dispersion in microchannels. *Applied Physics Letters* **88**, -, doi:doi:http://dx.doi.org/10.1063/1.2171797 (2006).

57 Das, A. J. & Narayan, K. S. Observation of Bessel beams from electric-field-induced patterns on polymer surfaces. *Opt. Lett.* **34**, 3391-3393, doi:10.1364/ol.34.003391 (2009).

58 Bag, M., Gupta, D., Arun, N. & Narayan, K. S. Deformation of metallic liquid drop by electric field for contacts in molecular–organic electronics. *Proceedings of the Royal Society A: Mathematical, Physical and Engineering Science* **465**, 1799-1808, doi:10.1098/rspa.2008.0460 (2009).

59 Padinger, F., Rittberger, R. S. & Sariciftci, N. S. Effects of Postproduction Treatment on Plastic Solar Cells. *Advanced Functional Materials* **13**, 85-88, doi:10.1002/adfm.200390011 (2003).

60 Zhao, C. X. *et al.* Organic photovoltaic power conversion efficiency improved by AC electric field alignment during fabrication. *Applied Physics Letters* **99**, -, doi:doi:http://dx.doi.org/10.1063/1.3623477 (2011).

61 Zhao, C. X. *et al.* Dual nanostructures in poly (3-hexylthiophene) based organic photovoltaics under alternative current electric field. *Thin Solid Films* **520**, 5770-5774, doi:http://dx.doi.org/10.1016/j.tsf.2012.04.079 (2012).

62 Ma, S.-Y., Shen, Y.-M., Yang, P.-C., Chen, C.-S. & Lin, C.-F. Morphological modification induced by external electric field during solution process of organic solar cells. *Organic Electronics* **13**, 297-301, doi:http://dx.doi.org/10.1016/j.orgel.2011.11.009 (2012).

63 Shen, Y.-M., Chen, C.-S., Yang, P.-C., Ma, S.-Y. & Lin, C.-F. Improvement of surface morphology of thin films and performance by applying electric field on P3HT:PCBM based solar cells. *Solar Energy Materials and Solar Cells* **99**, 263-267, doi:http://dx.doi.org/10.1016/j.solmat.2011.12.008 (2012).

64 Bagui, A. & Iyer, S. S. K. Effect of Solvent Annealing in the Presence of Electric Field on P3HT:PCBM Films Used in Organic Solar Cells. *Electron Devices, IEEE Transactions on* **58**, 4061-4066, doi:10.1109/ted.2011.2164545 (2011).

65 Bagui, A. & Iyer, S. S. K. in *Photovoltaic Specialists Conference (PVSC), 2012 38th IEEE.* 002301-002305.

Chapter 2

Materials and methods

2.1 Materials

For an efficient solar cell, right combinations of different materials are required. The different materials usually include donor molecules, acceptor molecules, solvents, additives, organic and inorganic buffer layers and electrodes. Each of them will be described in the next section. The materials chosen should have right orbital energies and should be processible into thin films..

2.1.1 Donor molecules

Donor molecules are organic materials in which the mobility for hole transport is higher. The materials used in this study are semiconducting polymers, where adjacent chains are held by VanderWaal's interaction. Hole mobility along a chain is faster than inter-chain hole-mobility due to the better overlap of wavefunction of electron within chains than between chains. The donor component of the active layer forms crystalline domains or amorphous regions depending upon the type of the donor used and their processing conditions. Most of the light absorbed in a solar cell is due to the donor component since they have high absorption coefficient and band-gap is tuned for absorption in visible – near IR energy region. The donor polymers used in the experiments were P3HT and PBDTTT-C-T.

2.1.1.1 P3HT

Poly(3-hexylthiophene-2,5-diyl) (P3HT) (Figure 2.1.a) is one of the widely studied donor materials[1-2]. The unit cell is a thiophene derivative. During polymerization, the thiophene units attaches with other thiophene units at its 3 and 5 positions. Regio-regular (RR) P3HT is one in which the units attach itself alternatively at 3 and 5 positions. This alternating arrangement of units provides RR-P3HT with higher degree of ordering between adjacent units. RR-P3HT has been found[3-5] to have mobilities as high as 0.1 cm^2/Vs due to its enhanced crystallinity .The HOMO of the polymer is around -5.2 eV, while LUMO lies around -3.2 eV. The band-gap of the polymer is about 1.9-2eV. P3HT absorbs between

400nm to 650nm with absorption maximum occurs around 540nm. Glass transition temperature is 12°C[6-7].RR-P3HT used in our experiments was bought from Luminescent Technologies.

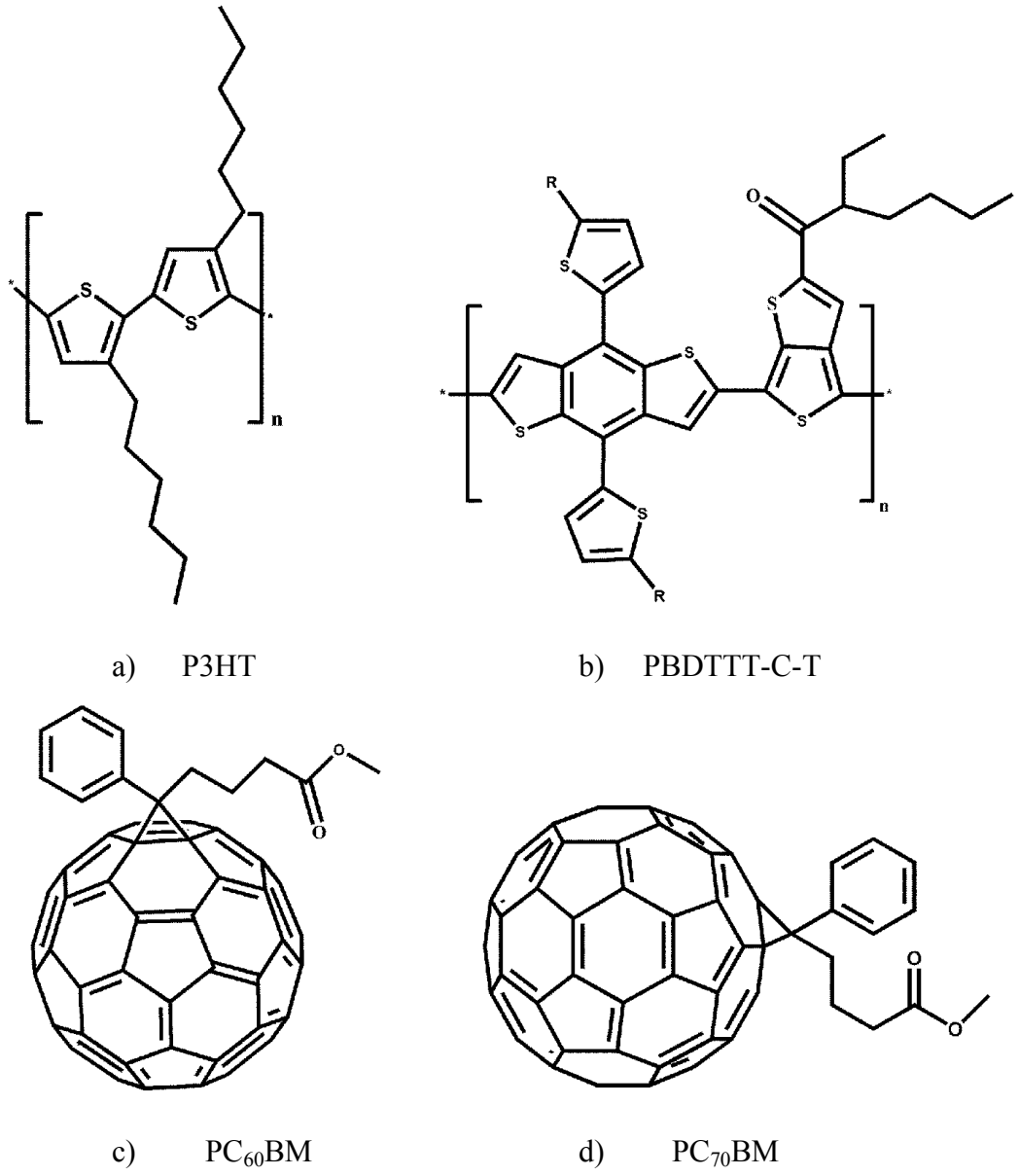

a) P3HT b) PBDTTT-C-T

c) $PC_{60}BM$ d) $PC_{70}BM$

***Figure 2. 1**: Donors and acceptors used*

2.1.1.2 PBDTTT-C-T

Most of the photons in the Infra-Red (IR) region are not absorbed by donors like P3HT. Lately, new amorphous donors having low band-gap increase absorption in the IR region and have come into prominence[8-10]. Poly([4,8-bis-ethyl-hexyl-thiophene-5-yl)-benzo[1,2-b : 4,5-b']dithiophene-2,6-diyl]-alt-[2-(2'-ethyl-hexanoyl)-thieno[3,4-b]thiophen-4,6-diyl]) (PBDTTT-C-T) (Figure 2.1.b) is one such low bandgap polymer with HOMO level placed at -5.11eV and LUMO level placed at -3.25eV. PBDTTT-C-T has a bandgap of 1.86eV. It absorbs between 500nm to 800nm with maximum around 700nm. Hole mobility[11] in PBDTTT-C-T is about 0.27 cm^2/Vs. PBDTTT-C-T used in this work was purchased from *Solarmer* Materials, Inc.

2.1.2 Acceptor molecules

Acceptor moleculess are organic materials in which the electron mobility is higher. They are usually small molecule systems. Fullerene based acceptors are most successful and commonly used acceptors[12]. Since they are easily processible and have optimum band levels, they make excellent candidates for solar cell fabrication with a range of donors. Due to the higher cost of fullerene acceptors, alternatives like perylene derivatives[13-14], twisted perylene[15], N2200 have been studied as substitutes in organic solar cells.

2.1.2.1 $PC_{60}BM$

[6,6]-phenyl-C_{61}-butyric acid methyl ester ($PC_{60}BM$) (Figure 2.1.c) is a small molecule derivative of fullerene[16]. This molecule which functions as an acceptor has its HOMO and LUMO around -6.0eV and -3.9eV respectively. This makes the molecule to have a bandgap of 2.1eV. The molecule absorbs in the wavelength range of 200nm to 400nm with absorption maximum around 270nm. Glass transition temperature of this molecule is found[6] to be 131.2^oC. Highest mobility reported[17] for $PC_{60}BM$ is 0.2 cm^2/Vs. $PC_{60}BM$ was purchased from MTR Ltd.

2.1.2.2 $PC_{70}BM$

Similar to $PC_{60}BM$, [6,6]-phenyl-C_{71}-butyric acid methyl ester ($PC_{70}BM$) (Figure 2.1.d) is also a bucky-ball small molecule which has its HOMO and LUMO levels at -5.8eV and -3.9eV respectively. It has a bandgap of 1.9eV. Solar cells with $PC_{70}BM$ as acceptor has

found to yield high open circuit voltage and higher efficiencies with donors like P3HT, PBDTTT-C-T, PCPDTBT[18-19]. Absorption range of this molecule is from 200nm to 400nm with maximum around 300nm. $PC_{70}BM$ was acquired from American Dye Source.

2.1.3 Buffer layers

Buffer layers are functional layers introduced between the active layer and electrodes to enhance charge extraction[20]. Layers are selected depending on their energy levels and carrier mobilities. They can be of organic or inorganic origin. Depending upon the carrier charge they allow, they are classified as electron buffer layer or hole buffer layer.

2.1.3.1 Hole buffer layer

The role of hole-conducting layers is to enhance hole collection efficiency at the anode. These layers block electron transport through them. The necessary criterion for a material to act as a hole-buffer layer is that its HOMO level should be intermediate between donor HOMO and the work function of the hole-collecting electrode.

PEDOT:PSS

Poly(3,4-ethylenedioxythiophene) poly(styrenesulfonate) (PEDOT:PSS) is one of the most commonly used solution-processable hole-buffer layers[21]. It is obtained as a colloidal suspension of PEDOT and PSS in water, where PSS is a stabilizer added during the polymerization of PEDOT. It is acidic in nature. Optimum thickness coated is 40-60 nm. This acts as a hole-conductor in normal structure devices. HOMO of PEDOT:PSS lies at -5.2eV.

MoO_3

Molybdenum Oxide is an inorganic hole-conducting buffer layer[22], which has HOMO around -5.3eV and LUMO around -2.4eV. This is usually thermal evaporated or solution processed. It has been shown[23] to improve long-term stability of the device when used as the hole-buffer layer. Optimum thickness used is 8.5nm. It is a common hole-buffer layer in inverted structure devices.

2.1.3.2 Electron Buffer layer

Electron buffer layers increases the efficiency of electron collection at cathode. They also act as hole blocking layers. The LUMO of the buffer layer should be close to the work-function of electron collecting electrode.

ZnO

Zinc Oxide is an electron buffer layer[24] for inverted devices. Its HOMO is at -7.5eV and LUMO is at -4.1eV. Usual thickness coated is around 40 nm. Initially, Zinc oxide films were coated from a solution of Zinc acetate and annealed at high temperatures. Recently, zinc oxide films coated from diluted nano dispersion has been found to perform better and does not require high temperature annealing. .

2.1.4 Additives

Addition of small volume of another high boiling solvent has found to increase the efficiency of solar cell. 1,8-di-iodo-octane(DIO)[25], alkyl-dithiols[26] are some of the commonly used additives. Additives have been found to enhance the performance of the device by selectively dissolving PCBM allowing more of P3HT in the other solvent, allowing P3HT to crystallize better. DIO can be removed by evaporating under high vacuum. We have used additive DIO in the fabrication of PBDTTT-C-T: $PC_{70}BM$ solar cells. The optimum volume percent of DIO in the solvent is 3%.

2.1.5 Electrodes

Electrodes of optimum work function are necessary for charge collection. Transparent ITO coated on glass acts as hole-collecting electrode in normal device structure and electron-collecting electrode in inverted device structure. Aluminium was used as electron collecting electrode in normal devices. Silver was the hole-collector in the inverted devices. The work functions of ITO, Aluminium and silver are -4.7eV, -4.1eV and -4.73eV respectively. ITO coated on glass is commercially available and act as substrates. Aluminium and silver are thermally deposited.

2.2 Processes involved in solar cell fabrication

The steps involved in the fabrication of solar cells are briefly discussed.

2.2.1 Etching of ITO

ITO coated slides are etched by dipping them in a diluted solution of aquaregia (3 parts of HCl to 1 part of HNO_3). More the dilution slower the etching and hence better the control. Care should be taken to avoid vapours of aquaregia interacting with the ITO which we do not want to get etched.

2.2.2 RCA treatment

This treatment is usually done to clean substrates (glass or ITO). The slides are initially cleaned in IPA-acetone solution and blow dried with air gun. Measured volume of de-ionized water is pre-heated in a petridish to around 90^{o}C, ammonia solution and hydrogen peroxide are added such that the volume ratio of water, ammonia solution and hydrogen peroxide are 5:1:1.The substrates are placed in the bubbling solution. For ITO substrates, the conducting side is kept facing up. After 5-10 min of RCA treatment, the substrates are transferred to de-ionized water and sonicated for 5 min followed by blow-drying.

Figure 2. 2: *Etching of ITO*

2.2.3 Thermal deposition

Top electrodes and some buffer layers like molybdenum oxide are coated by thermal deposition. The masked samples are initially held onto to the substrate holder. The required quantities of metal/compound are then loaded onto boats (coil/basket). The chamber is sealed and vacuum is created using rotary and turbo pump. The metal/compound parameters like density and acoustic impedence are entered in film thickness monitor. When the pressure is

down to $5*10^{-6}$ mbar, current is passed through the boat, which evaporates the metal/compound. The rate of coating can be controlled by the current applied. The thickness coated is monitored by a crystal oscillator based thickness monitor. Initially the rate of coating is maintained < 1 nm/s. Rate is increased as the coating proceeds. The samples are allowed to cool down for 2 hours after coating is done.

2.3 Characterization of an organic Solar cell

The experiments used to characterize OSCs are;

1. Current Density – Voltage measurement (J-V curve)
2. Incident Photon to Converted Electron ratio measurement(IPCE)
3. Atomic Force Microscopy

2.3.1 Current density – voltage measurement

Solar cells are characterized by applying voltage and measuring current collected flowing through the device. Under dark conditions, the device acts like a diode. The current through the device in the reverse bias is much less as exhibited in a p-n junction. The current increases in the forward bias, and follows an exponential trend above a threshold voltage. Under light, there is a large amount of photo-generated carriers in the active layer. These photo-generated carriers are extracted at their respective electrodes. For an efficient device, the current almost remains constant in the reverse bias regime. The current flowing through the device when the external voltage is zero is called short-circuit current, J_{sc}. In the forward bias regime, the current value increases and becomes zero at a particular voltage value, which is referred to as open-circuit voltage, V_{oc}. The point in the J-V curve when the product of voltage and current density is largest is called the maximum power point (P_{max}). Voltage at the corresponding P_{max} is coined V_{max} and current density at the P_{max} is called J_{max}.

Fill factor is defined as the ratio of P_{max} and the product of V_{oc} and J_{sc}. Efficiency of the solar cell (η) is given by

$$\eta = \frac{FF * V_{oc} * J_{sc}}{P_{in}} \quad \text{.....(4)}$$

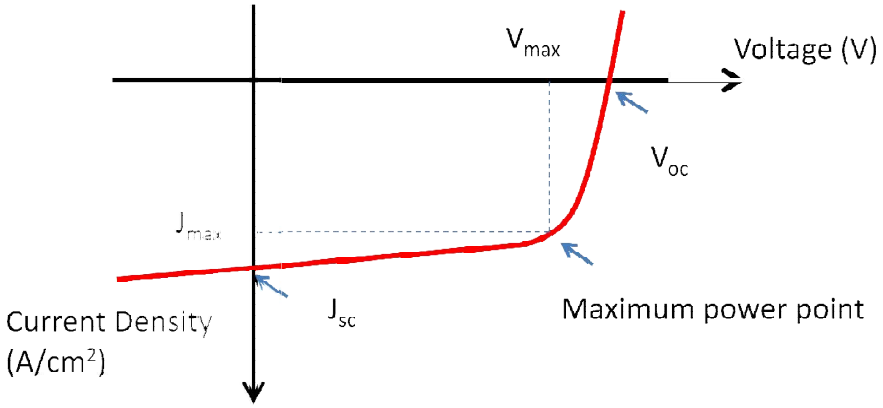

Figure 2. 3: *Current density - voltage characteristics of a solar cell*

This characterization technique provides us with short circuit current (J_{sc}), open circuit voltage (V_{oc}), fill factor, efficiency, shunt resistance and series resistance of the device.

Experimental setup consists of Four-Probe setup with two leads sweeping the voltage and other two leads measuring voltage applied across the device using a Source Meter (Keithley 2420). The exposure duration and the rate of sweeping of voltage can be controlled. Source Meter is interfaced with the corresponding data acquisition software. (Oriel Instruments I-V test station)

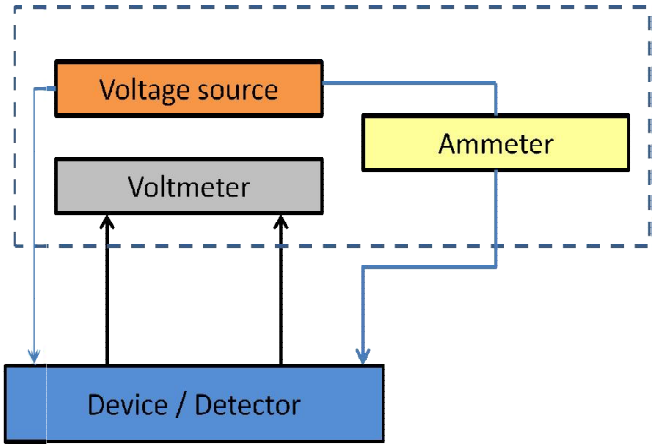

Figure 2. 4: *Schematic diagram of J-V measurement setup*

Light intensity of 100 mW/cm^2 and Sun spectrum of AM 1.5 Global (IEC 904-3) which is an international standard for incident light used in J-V measurement was used in all the

measurements. Light spectrum was provided by the solar simulator (Newport class AAA solar simulator). The power was calibrated every time before measurement.

J-V characterization was done by sweeping the source voltage from 1.0V to -0.5V with 200 sweep points between them. Dark current scan is run initially for each of the device, followed by the current scan under 1 sun illumination. The exposure time for current scan under light is about 11 seconds.

2.3.2 IPCE measurement

IPCE is analogous to EQE. IPCE is defined as the ratio of the number of electrons collected at the interface to the number of photons incident on the device as a function of wavelength.

$$IPCE(\lambda) = \frac{n_{electrons-collected}}{n_{photons-absorbed}} = \frac{J*1240}{P*\lambda} \quad \ldots\ldots\ldots\ldots\ldots\ldots\ldots\ldots\ldots\ldots\ldots\ldots\ldots\ldots(1)$$

Here J is the short circuit current density in A/cm^2, P is incident light power in W/cm^2. λ is wavelength in nanometer. IPCE can tell us about the efficiency of photon to electron conversion at different wavelengths. It is usually expressed in percentage, by after multiplying the right hand side of the above equation by 100.

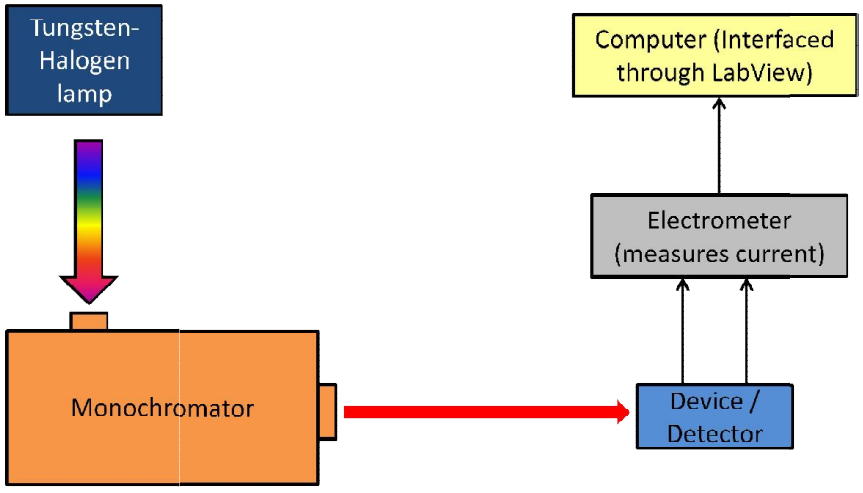

***Figure 2. 5**: Schematic diagram of IPCE measurement setup*

The experimental setup consists of a light source (Zolix LSH – T150 Tungsten Halogen Lamp) coupled with a monochromator (SPEX 500). The spectral width of output light from the monochromator is controlled through a slit, a pinhole of diameter 1mm is used to keep

the illumination are in device/detector constant. Device is measured under short circuited condition . The current output is measured using Electrometer (Kiethley EM 6514) which is interfaced with the computer using LabView 2011 program. The power intensity is calibrated using a calibrated silicon detector. Detector used in our experiments was silicon detector from UDT instruments. P is obtained by dividing J_{sc} of the detector at each wavelength by the corresponding responsity (A/W) of the detector at each of the wavelength. Area normalization is done by keeping the detector in the same place as the device. IPCE is run by sweeping the wavelength between 400nm to 800 nm, with steps of 2nm. Time delay at each step is kept at 2 seconds.

2.3.3 Atomic force microscopy (AFM)

AFM was used to study the surface morphology of the OPV devices. JPK Instruments (Nanowizard 3) AFM was used in this study, the AFM head is mounted on an inverted microscope (Carl-Zeiss). Feedback is controlled using Four-Quadrant position detector measuring the deflection of the 810 nm laser from the AFM cantilever as the tip scans over the surface.

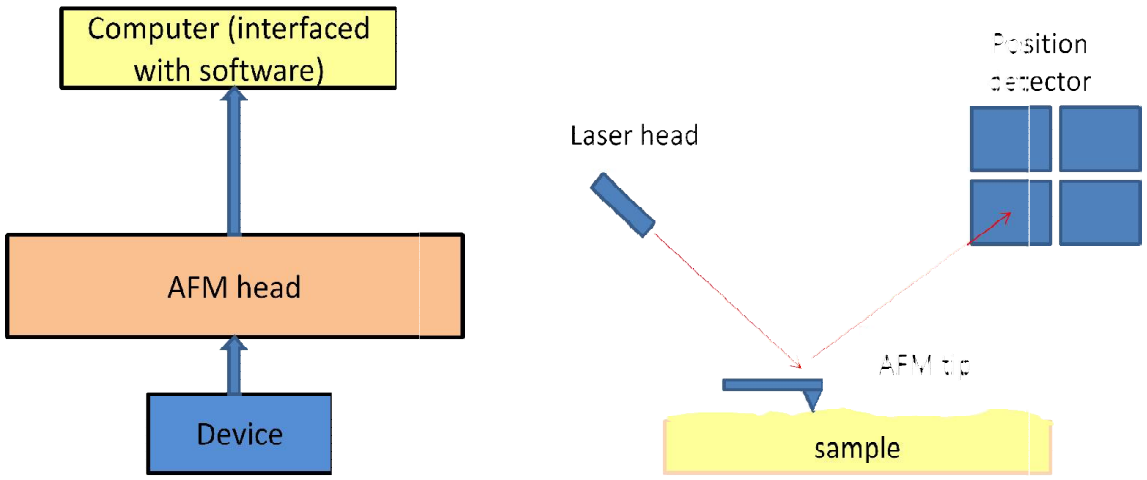

Figure 2. 6: *Schematic diagram of AFM arrangement for surface studies on the device*

The topography images can give information about the roughness of the semiconducting surface. Apart from the topographic variations of the surface, AFM used in tapping mode gives information about the phase segregation in binary system like BHJ. Different regions (donors and acceptors domains) have characteristic phase contrast. By mapping out the

different phase contrast on the film surface, the acceptor and donor domains could be mapped.

2.4 References

1 Dang, M. T., Hirsch, L. & Wantz, G. P3HT:PCBM, Best Seller in Polymer Photovoltaic Research. *Advanced Materials* **23**, 3597-3602, doi:10.1002/adma.201100792 (2011).

2 Liu, C.-Y., Holman, Z. C. & Kortshagen, U. R. Hybrid Solar Cells from P3HT and Silicon Nanocrystals. *Nano Letters* **9**, 449-452, doi:10.1021/nl8034338 (2008).

3 Sirringhaus, H., Tessler, N., Thomas, D. S., Brown, P. J. & Friend, R. H. in *Advances in Solid State Physics 39* Vol. 39 *Advances in Solid State Physics* (ed Bernhard Kramer) Ch. 9, 101-110 (Springer Berlin Heidelberg, 1999).

4 Sirringhaus, H., Tessler, N. & Friend, R. H. Integrated Optoelectronic Devices Based on Conjugated Polymers. *Science* **280**, 1741-1744, doi:10.1126/science.280.5370.1741 (1998).

5 Wang, G., Swensen, J., Moses, D. & Heeger, A. J. Increased mobility from regioregular poly(3-hexylthiophene) field-effect transistors. *Journal of Applied Physics* **93**, 6137-6141, doi:doi:http://dx.doi.org/10.1063/1.1568526 (2003).

6 Zhao, J. *et al.* Phase Diagram of P3HT/PCBM Blends and Its Implication for the Stability of Morphology. *The Journal of Physical Chemistry B* **113**, 1587-1591, doi:10.1021/jp804151a (2009).

7 Zhao, Y., Yuan, G., Roche, P. & Leclerc, M. A calorimetric study of the phase transitions in poly(3-hexylthiophene). *Polymer* **36**, 2211-2214, doi:http://dx.doi.org/10.1016/0032-3861(95)95298-F(1995).

8 Bundgaard, E. & Krebs, F. C. Low band gap polymers for organic photovoltaics. *Solar Energy Materials and Solar Cells* **91**, 954-985, doi:http://dx.doi.org/10.1016/j.solmat.2007.01.015 (2007).

9 Kroon, R., Lenes, M., Hummelen, J. C., Blom, P. W. M. & de Boer, B. Small Bandgap Polymers for Organic Solar Cells (Polymer Material Development in the Last 5 Years). *Polymer Reviews* **48**, 531-582, doi:10.1080/15583720802231833 (2008).

10 Chen, H.-Y. *et al.* Polymer solar cells with enhanced open-circuit voltage and efficiency. *Nat Photon* **3**, 649-653 (2009).

11 Huo, L. *et al.* Replacing Alkoxy Groups with Alkylthienyl Groups: A Feasible Approach To Improve the Properties of Photovoltaic Polymers. *Angewandte Chemie International Edition* **50**, 9697-9702, doi:10.1002/anie.201103313 (2011).

12 Zhang, F. *et al.* Influence of PC60BM or PC70BM as electron acceptor on the performance of polymer solar cells. *Solar Energy Materials and Solar Cells* **97**, 71-77, doi:http://dx.doi.org/10.1016/j.solmat.2011.09.006 (2012).

13 Shin, W. S. *et al.* Effects of functional groups at perylene diimide derivatives on organic photovoltaic device application. *Journal of Materials Chemistry* **16**, 384-390, doi:10.1039/b512983d (2006).

14 Anthony, J. E. Small-Molecule, Nonfullerene Acceptors for Polymer Bulk Heterojunction Organic Photovoltaics†. *Chemistry of Materials* **23**, 583-590, doi:10.1021/cm1023019 (2010).

15 Shivanna, R. *et al.* Charge generation and transport in efficient organic bulk heterojunction solar cells with a perylene acceptor. *Energy & Environmental Science* **7**, 435-441, doi:10.1039/c3ee42484g (2014).

16 Roncali, J. Linear [small pi]-conjugated systems derivatized with C60-fullerene as molecular heterojunctions for organic photovoltaics. *Chemical Society Reviews* **34**, 483-495, doi:10.1039/b415941c (2005).

17 Singh, T. B. *et al.* Fabrication and characterization of solution-processed methanofullerene-based organic field-effect transistors. *Journal of Applied Physics* **97**, -, doi:doi:http://dx.doi.org/10.1063/1.1895466 (2005).

18 Ratcliff, E. L. *et al.* Energy level alignment in PCDTBT:PC70BM solar cells: Solution processed NiOx for improved hole collection and efficiency. *Organic Electronics* **13**, 744-749, doi:http://dx.doi.org/10.1016/j.orgel.2012.01.022 (2012).

19 Adhikary, P. *et al.* Enhanced charge transport and photovoltaic performance of PBDTTT-C-T/PC70BM solar cells via UV-ozone treatment. *Nanoscale* **5**, 10007-10013, doi:10.1039/c3nr03355d (2013).

20 Po, R., Carbonera, C., Bernardi, A. & Camaioni, N. The role of buffer layers in polymer solar cells. *Energy & Environmental Science* **4**, 285-310, doi:10.1039/c0ee00273a (2011).

21 Kang, N. S. *et al.* Partitioning of the organic layers for the fabrication of high efficiency organic photovoltaic devices. *Organic Electronics* **10**, 1091-1096, doi:http://dx.doi.org/10.1016/j.orgel.2009.05.021 (2009).

22 Tao, C. *et al.* Performance improvement of inverted polymer solar cells with different top electrodes by introducing a MoO3 buffer layer. *Applied Physics Letters* **93**, -, doi:doi:http://dx.doi.org/10.1063/1.3026741 (2008).

23 Yamanari, T., Taima, T., Sakai, J., Tsukamoto, J. & Yoshida, Y. Effect of Buffer Layers on Stability of Polymer-Based Organic Solar Cells. *Japanese Journal of Applied Physics* **49**, 01AC02.

24 White, M. S., Olson, D. C., Shaheen, S. E., Kopidakis, N. & Ginley, D. S. Inverted bulk-heterojunction organic photovoltaic device using a solution-derived ZnO underlayer. *Applied Physics Letters* **89**, -, doi:doi:http://dx.doi.org/10.1063/1.2359579 (2006).

25 Lee, J. K. *et al.* Processing Additives for Improved Efficiency from Bulk Heterojunction Solar Cells. *Journal of the American Chemical Society* **130**, 3619-3623, doi:10.1021/ja710079w (2008).

26 Peet, J. *et al.* Efficiency enhancement in low-bandgap polymer solar cells by processing with alkane dithiols. *Nat Mater* **6**, 497-500, doi:http://www.nature.com/nmat/journal/v6/n7/suppinfo/nmat1928_S1.html (2007).

Chapter 3

Electric field assisted solvent drying in P3HT: $PC_{60}BM$ solar cells

3.1 P3HT:$PC_{60}BM$ BHJ system

P3HT:$PC_{60}BM$ is one of the most widely studied BHJ blends[1-5], whose characteristics depends on donor to acceptor ratio, molecular weight of P3HT[6], regio-regularity[7] of P3HT, solvent used and annealing treatments[8]. By careful optimization, efficiencies higher than 5% have been reported[9] for this system. The reasons for the high performance of P3HT: $PC_{60}BM$ include

i) The higher absorption coefficient ($\alpha \sim 10^5$ cm^{-1}) and band-gap (~1.9eV) for the P3HT, helps in absorbing most of the visible part of solar spectrum.

ii) Optimal difference between LUMO of donor and acceptor, which gives sufficient driving force for charge transfer.

iii) V_{oc} (~600mV) provided by the difference P3HT-HOMO and $PC_{60}BM$-LUMO

iv) Comparable hole and electron mobilities in the donor and acceptor respectively.

3.1.1 Device

P3HT:$PC_{60}BM$ solar cells used in our experiments were of inverted structure with ZnO as the electron buffer layer and MoO_3 as the hole buffer layer. ITO and silver acts as the electron collecting and hole collecting electrodes respectively. The zinc oxide buffer layer was made from two different sources, zinc acetate solution (referred to as 'ZnO sol') and from diluted solution of zinc oxide nanoparticle dispersion (referred to as 'ZnO NP')

3.1.2 P3HT:$PC_{60}BM$ solution preparation

The optimum blend ratio[1] for P3HT: $PC_{60}BM$ is 1:1, with 10 mg/ml of polymer and 10 mg/ml of $PC_{60}BM$ in chlorobenzene. The solution was stirred overnight at 60^oC before use.

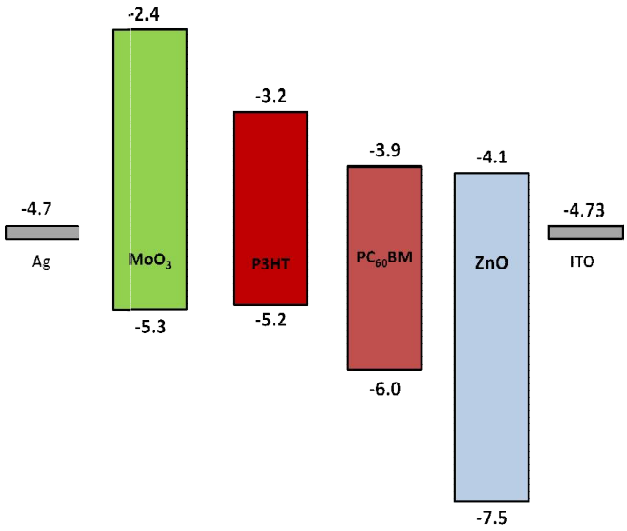

***Figure 3. 1**: The band levels of ITO/ZnO/P3HT: $PC_{60}BM/MoO_3$/Ag. The numerical values in the image are electron energy values in eV.*

3.1.3 ZnO sol preparation

314 mg of zinc acetate was mixed with 3.14 mL of 2-methoxy ethanol and 86 µL of ethanolamine. The solution was stirred at 60°C for 10 mins. A transparent solution was obtained. The solution was spin coated at 2000 rpm on RCA treated ITO glass plates and annealed at 250°C for 30 minutes.

3.1.4 ZnO NP preparation

60 µL of the original nano-dispersion solution (40 wt% of ZnO nanoparticles in ethanol) was diluted with 2.94mL of ethanol to make 3 mL of ZnO nanoparticle dispersion (2vol% of the original solution). The dispersion was then stirred at 60°C for 10 minutes for homogeneity. The solution was then spin coated and annealed at 100°C for 10 minutes.

3.2 Active layer

3.2.1 Fabrication of polymer thin film

The active layer was spin-coated on the ZnO buffer layer within a glove box environment (O_2 ~ 1 ppm, H_2O < 1 ppm). The films were then thermally annealed (TA) or thermally annealed in electric field or left un-annealed (UA). Physical masks of 3mm active area were placed on the polymer layer. 8-8.5nm of MoO_3 and 100 nm of Ag was evaporated using vacuum thermal deposition.

3.2.2 Thermal annealing of active layer

As discussed in the earlier chapter, thermal annealing has been found to increase the performance of P3HT:$PC_{60}BM$ solar cells due to the phase segregation of the donor and acceptor species. After spin-coating of the polymer BHJ layer in the glove box, the cell was heated slowly from room temperature to 120^{o}C, where it was allowed to stay for 5 minutes and then was slowly cooled to room temperature.

3.2.3 Thermal annealing of active layer in electric field

While annealing the active layer, electric field (~ 10^7 V/m) was applied between ITO and a non contacting top electrode. The top electrode was made using ITO glass (with its conducting side facing towards active layer) which was separated from the active layer by ~ 100 μm using a spacer (strips of PTFE tape). A constant DC voltage of 300V was applied by a high voltage supply (Keithley model 248) during the annealing process. The setup used is shown in figure 3.2.

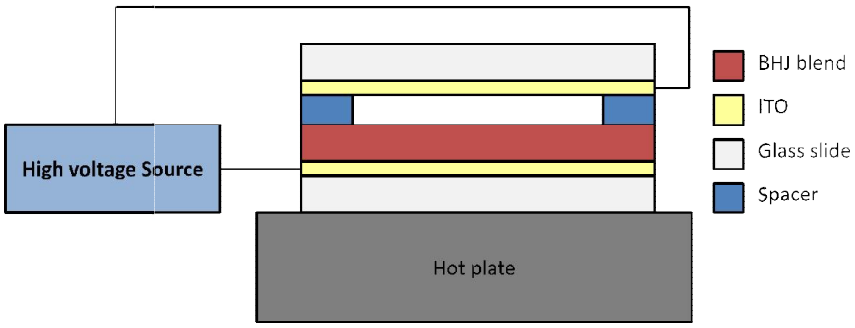

Figure 3.2: *Schematic of experimental setup for thermal-annealing-in-electric-field of the samples*

In every batch, un-annealed (UA), thermally annealed (TA) and thermal annealed-in-electric field (TAIE) solar cells were fabricated.

3.3 Organic solar cell characterization

3.3.1 Solar cell based on zinc acetate buffer layer

These solar cells have zinc oxide prepared from zinc acetate as the electron buffer layer.

3.3.1.1 J-V characterization

	Treatment	Voc (V)	Jsc (mA/cm^2)	Fill Factor	Efficiency
Average	UA	0.64	3.70	31.61	0.69
	TA	0.57	8.55	49.50	2.22
	TAIE	0.58	9.71	54.86	2.88
Best	UA	0.67	4.17	31.87	0.81
	TA	0.57	10.10	51.91	2.72
	TAIE	0.60	11.22	60.28	3.70

Table 3. 1: *Average and best of device performance of ITO/ZnO(Sol)/P3HT:$PC_{60}BM$/MoO_3/Ag under different treatments.*

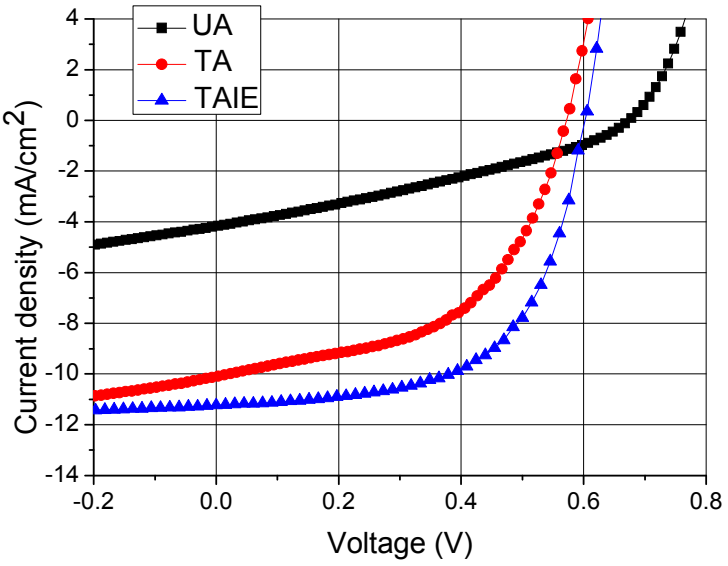

Figure 3. 3: *J-V characteristics of best devices under different treatments for ITO/ZnO (Sol)/P3HT:$PC_{60}BM$/MoO_3/Ag samples*

Table 3.1 shows the result for average (~ 5 devices in each set) and best performing P3HT:$PC_{60}BM$ solar cells. Comparing between UA and TA samples, it can be seen that there

is a siginificant improvement in short circuit current density (J_{sc}), fill factor (FF) and power conversion efficiency (η) upon annealing. This is due to the crystallization of P3HT during annealing. Though there is a small decrease in V_{oc}, increase in J_{sc} and fill factor, reflects itself as increase in efficiency.

Annealing under electric field further improves V_{oc}, J_{sc} and FF, which subsequently shows up in efficiency. The best device showed efficiency as high as 3.7% with J_{sc} > 11 mA/cm^2, as shown in the table. Overall, on average, percentage increase in J_{sc}, FF, η on electric field annealing over thermal annealing was 14%, 11% and 30% respectively. It can be observed that there is an enhancement in J_{sc} in TAIE samples of all batches.

P3HT being a crystalline donor, it is expected that the electric field induces dipole moment in them. This induced dipole moment would help the adjacent units to align with it. This helps in better crystallization of P3HT and extended connectivity in P3HT. This enhanced connectivity increases carrier transport in the film. This is further evident in AFM studies (discussed in section 3.3.2.3).Thus without compromising the interface area required for charge separation, better charge transport and charge collecting has been made possible through thermal annealing along with the external electric field. Since electric field is maintained when the system is cooled down, the film assumes the frozen morphology. The film morphology of TAIE samples is different from the film morphology of TA samples.

3.3.2 Solar cell based on ZnO nano dispersion buffer layer

In these solar cells, the electron buffer layer was prepared from ZnO nanoparticle dispersion instead of Zinc acetate solution. It has been reported[10] that devices using buffer layer deposited from ZnO nanoparticle dispersion gives efficiency higher as compared to zinc acetate based buffer layer. The films obtained using ZnO NP's was visible smooth with no particulates. Moreover films prepared from ZnO NP required annealing at 100^{o}C for 10 minutes as compared to ZnO Sol which requires annealing at 250^{o}C for 30 minutes.

3.3.2.1 J-V characterization:

	Treatment	Voc (V)	Jsc (mA/cm^2)	Fill Factor	Efficiency
Average	UA	0.64	3.14	37.62	0.69
	TA	0.55	7.27	50.90	1.85
	TAIE	0.56	7.64	52.44	2.07
Best	UA	0.65	3.33	39.65	0.78
	TA	0.59	7.88	56.40	2.40
	TAIE	0.59	9.42	56.02	2.81

Table 3. 2: *Average and best of device performance of ITO/ZnO (NP)/P3HT:$PC_{60}BM$/MoO_3/Ag under different treatments*

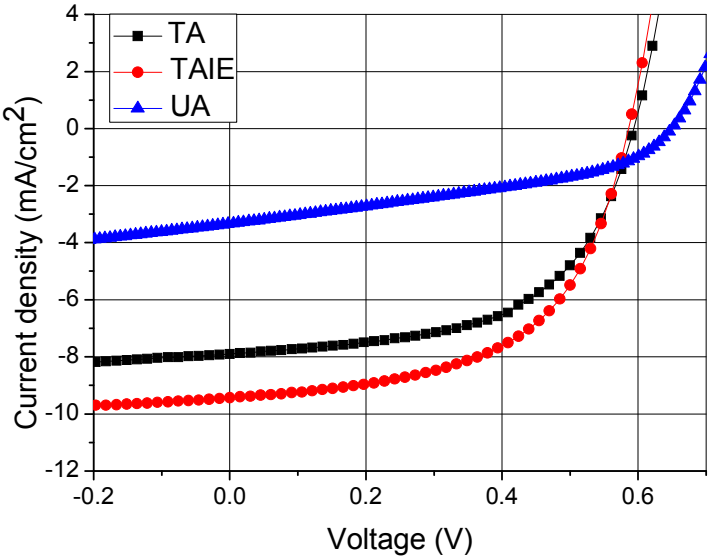

Figure 3. 4: *J-V characteristics of best devices under different treatments for ITO/ZnO (NP)/P3HT:$PC_{60}BM$/MoO_3/Ag samples*

The table 3.2 summarizes the results for average (~ 5 devices in each set) and best devices; figure 3.4 shows the J-V characteristics for three different treatments to semiconducting layer. Comparing the device performance of ZnO sol-based OSCs with ZnO NP-based OSCs, it can be noticed that the J_{sc} values were lower for the latter. Further optimization in film thickness and annealing procedures are required to increase J_{sc}. Device performance was

found to be best for TAIE samples. Their percentage increase in the average values of J_{sc}, FF and efficiencies are found to be 5%, 3% and 11% respectively, when compared with TA samples.

3.3.2.2 IPCE

The IPCE spectrum shown in figure 3.5 shows significant enhancement for TA and TAIE samples. The absorption increases throughout the spectrum, which reflects in the increase in J_{sc}, since area under the IPCE curve is equivalent to J_{sc}. The $IPCE_{max}$ for UA, TA and TAIE is 29% 496nm), 46% (488nm) and 52% (484nm) respectively.

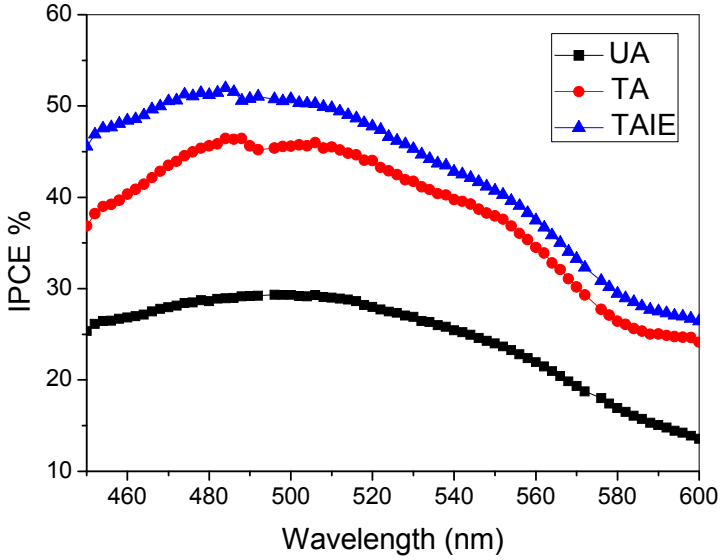

Figure 3. 5: *IPCE spectrum of ITO/ZnO (NP)/P3HT:$PC_{60}BM$/MoO_3/Ag under different treatments*

3.3.2.3 AFM results

In this section the topographic and phase images obtained through AFM, for UA, TA and TAIE solar cells of ITO/ (ZnO NP) /P3HT:$PC_{60}BM$ /MoO_3/Ag geometry has been discussed. Active layer was mapped in between the top electrodes.

a) UA:

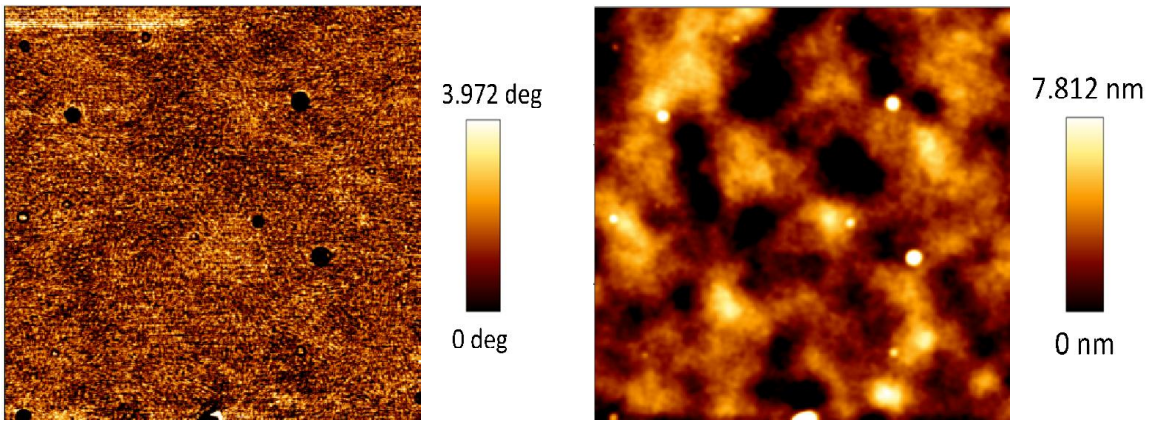

a) Phase-image of 3µm X 3µm scan b) Topographic image of 3µm X 3µm scan

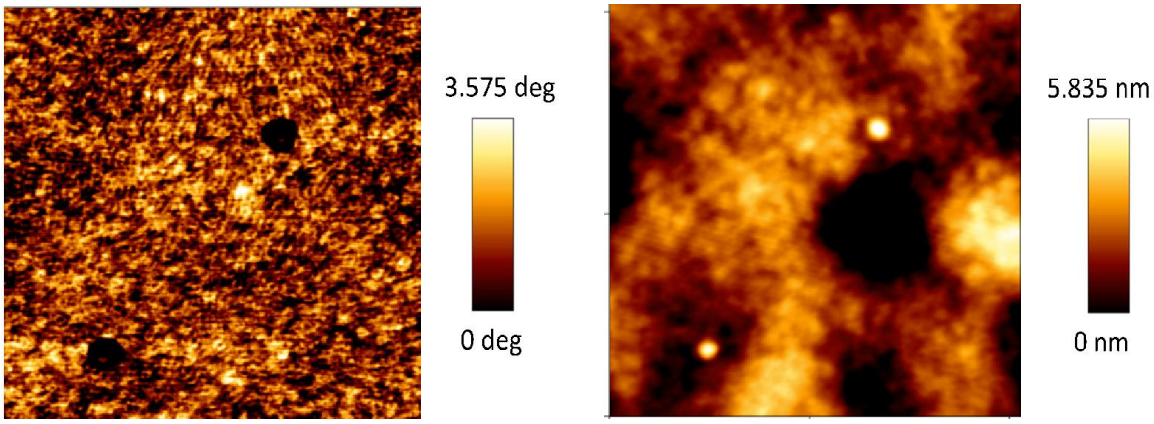

c) Phase-image of 1µm X 1µm scan d) Topographic image of 1µm X 1µm scan

Figure 3. 6: *AFM phase image and topographic images of un-annealed (UA) samples*

Figure 3.6 shows the phase and topography image for UA cells. The phase images ((3.6 a) and (3.6 c)) of the UA samples show that the phase segregation of P3HT and $PC_{60}BM$ domains is not present. This results in low J_{sc} (~ 3 mA/cm^2) and low FF (~30%). The topographic image shows that the film is very smooth. $RMS_{roughness}$ of the images (3.6 b) and (3.6 d) are ~ 1.5nm.

(b)TA:

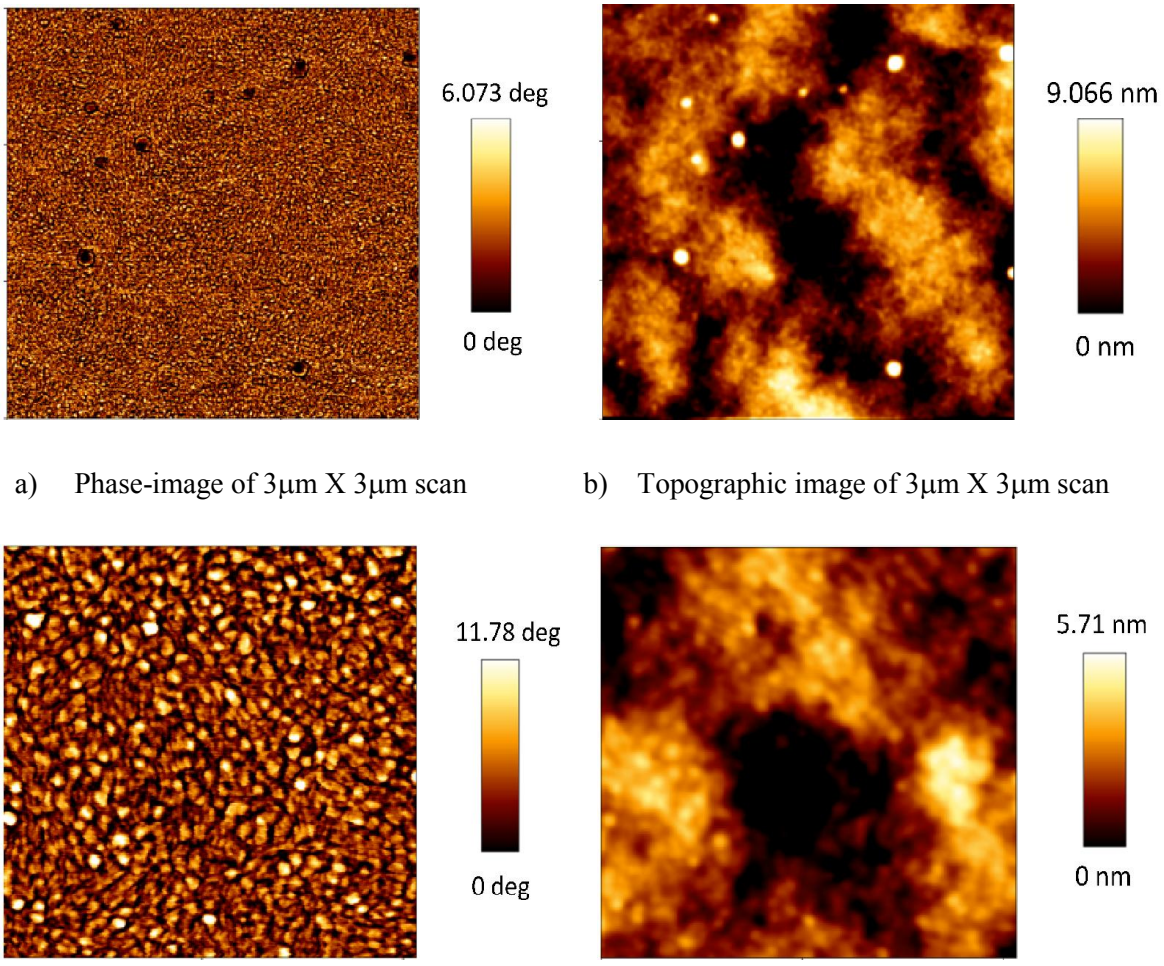

a) Phase-image of 3µm X 3µm scan

b) Topographic image of 3µm X 3µm scan

c) Phase-image of 1µm X 1µm scan

d) Topographic image of 1µm X 1µm scan

Figure 3. 7: *AFM phase image and topographic images of thermally annealed (TA) samples*

Figure 3.7 shows the phase and topography image for TA cells. The phase images clearly show a well phase segregated regions when compared with UA images. From the phase image (3.7 c), we can clearly distinguish domains of pure donor/ acceptor. The dimension of the domains are on average are around 20-40nm. Better optimization of domain connectivity and charge generation interface area increases J_{sc} (~7.88 mA/cm^2) and Fill factor (~56). Topographic images reveal a $RMS_{roughness}$ of ~ 2 nm.

(c) TAIE:

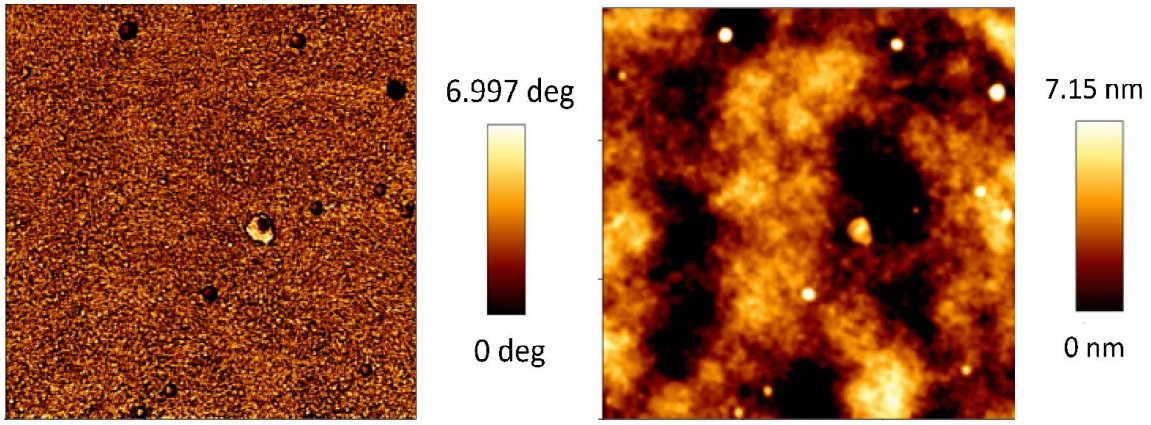

a) Phase-image of 3µm X 3µm scan b) Topographic image of 3µm X 3µm scan

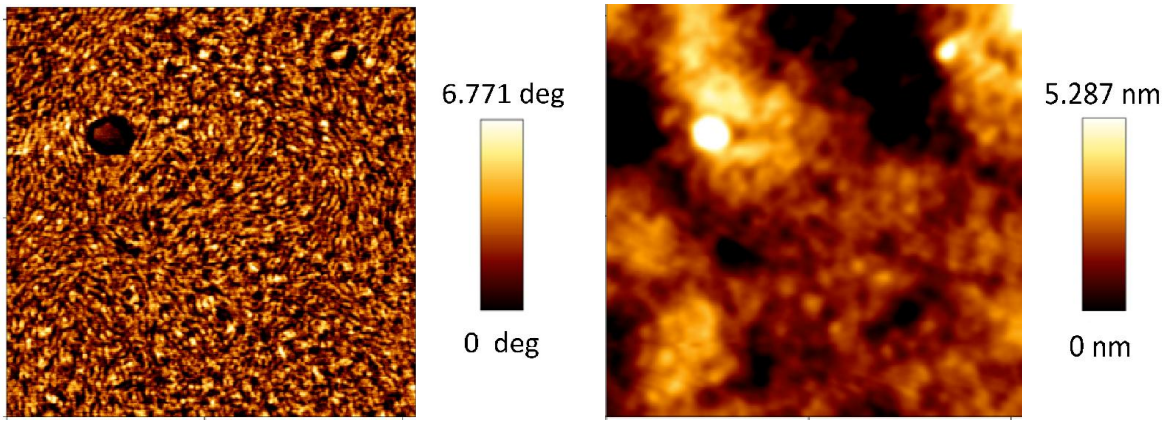

c) Phase-image of 1µm X 1µm scan d) Topographic image of 1µm X 1µm scan

Figure 3. 8: *AFM phase image and topographic images of thermally annealed samples in Electric field (TAIE) samples*

Figure 3.8 shows the phase and topography image for TAIE cells. The phase images shows that phase segregation of the domains and a better oriented interconnection of P3HT chains. Without compromising on the interface area for charge separation, charge carrier pathways are created due to annealing in electric field. The FF is same as that of the annealed samples (~56). Since better interconnected pathways reduces non-geminate recombination of the separated charges, J_{sc} increases (~9.4 mA/cm^2). $RMS_{roughness}$ of the topographic images b) and d) are ~1.5nm indicating smooth film formed.

3.4 Discussion

In summary, thermal annealing in electric field appears to improve device performance. A qualitative picture of electric field induced effects is depicted in the figure 3.9

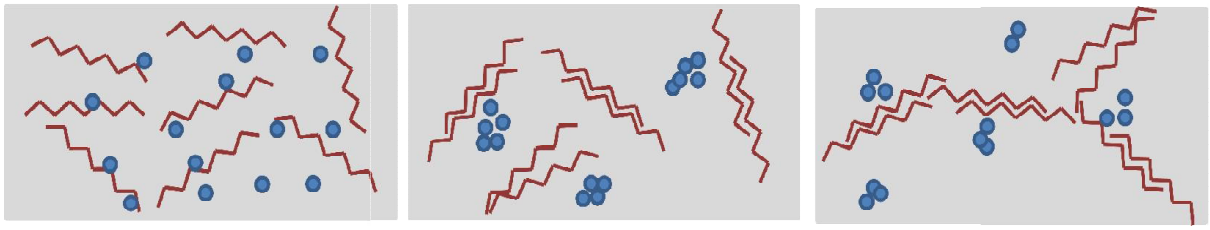

(a) UA *(b)TA* *(c)TAIE*

Figure 3. 9: *Schematic representation of the film morphology of P3HT: $PC_{60}BM$ OSCs when the samples are un-annealed (a), thermally annealed (b), thermally annealed in electric field (c).The red coloured strips indicate P3HT chains and blue circles indicate PCBM.*

From the characterization techniques used to understand solar cells, we realize that for the UA case, there is minimal phase segregation. Though there is a relatively large contact interfaces between P3HT and $PC_{60}BM$, the separated charges do not reach the collecting electrodes. This is evident from the phase images of AFM and low J_{sc} values.

For the TA samples, due to the increase in diffusion of $PC_{60}BM$ molecules at higher temperatures, tendency to from nanocrystalline domains enhances along with self assembly of $PC_{60}BM$. The phase segregated pure domains of P3HT and $PC_{60}BM$ thus formed can be observed in AFM images, Increase in interface area, along with better interconnected charge transport pathways can possibly lead to higher J_{sc} and FF for these devices.

For TAIE samples, an optimum phase separation in P3HT and $PC_{60}BM$ has been achieved. It is expected that the induced dipole moment, in presence of electric field, favours better alignment with neighboring chains, leading to a better oriented connectivity between P3HT chains. J_{sc} of TAIE samples are higher than TA samples. Since the induced dipole moment is not large in P3HT, alignment is persistent over small scales. Due to sphericity of $PC_{60}BM$, the acceptor species are not expected to have sufficient dipole moment for alignment.

3.5 Conclusion and future directions

In P3HT based solar cells, better optimization for cells with ZnO NP buffer layer has to be done. It is clearly evident that electric field during annealing plays a role in controlling the device morphology and performance. By varying the electric field, better enhancement could be achieved. Applying electric field only, without thermal annealing, should help us to deconvolute the role played by electric field and thermal annealing, in forming a better morphology. Using different acceptors with P3HT can help us understand the role played by acceptor in these scenarios. OSCs with $PC_{70}BM$ as acceptor, with and without addition of additives and annealing in electric field will be studied. Evaporation of solvent in vacuum and electric-field during vacuum evaporation of solvent could be explored for P3HT donor based OSCs.

3.6 References

1 Dang, M. T., Hirsch, L., Wantz, G. & Wuest, J. D. Controlling the Morphology and Performance of Bulk Heterojunctions in Solar Cells. Lessons Learned from the Benchmark Poly(3-hexylthiophene):[6,6]-Phenyl-C61-butyric Acid Methyl Ester System. *Chemical Reviews* **113**, 3734-3765, doi:10.1021/cr300005u (2013).

2 Kim, J. Y. *et al.* New Architecture for High-Efficiency Polymer Photovoltaic Cells Using Solution-Based Titanium Oxide as an Optical Spacer. *Advanced Materials* **18**, 572-576, doi:10.1002/adma.200501825 (2006).

3 Thompson, B. C. & Fréchet, J. M. J. Polymer–Fullerene Composite Solar Cells. *Angewandte Chemie International Edition* **47**, 58-77, doi:10.1002/anie.200702506 (2008).

4 Brabec, C. J. & Durrant, J. R. Solution-Processed Organic Solar Cells. *MRS Bulletin* **33**, 670-675, doi:doi:10.1557/mrs2008.138 (2008).

5 Li, G. *et al.* High-efficiency solution processable polymer photovoltaic cells by self-organization of polymer blends. *Nat Mater* **4**, 864-868 (2005).

6 Yasuda, T., Meguro, H., Okamoto, S. & Han, L. Bulk-heterojunction organic photovoltaic cells fabricated using a high-viscosity solution of poly(3-hexylthiophene) with extremely high molecular weight. *Polym J* **45**, 129-132 (2013).

7 Kim, Y. *et al.* A strong regioregularity effect in self-organizing conjugated polymer films and high-efficiency polythiophene:fullerene solar cells. *Nat Mater* **5**, 197-203, doi:http://www.nature.com/nmat/journal/v5/n3/suppinfo/nmat1574_S1.html (2006).

8 Li, G., Shrotriya, V., Yao, Y., Huang, J. & Yang, Y. Manipulating regioregular poly(3-hexylthiophene) : [6,6]-phenyl-C61-butyric acid methyl ester blends-route towards high efficiency polymer solar cells. *Journal of Materials Chemistry* **17**, 3126-3140, doi:10.1039/b703075b (2007).

9 Irwin, M. D., Buchholz, D. B., Hains, A. W., Chang, R. P. H. & Marks, T. J. p-Type semiconducting nickel oxide as an efficiency-enhancing anode interfacial layer in polymer

bulk-heterojunction solar cells. *Proceedings of the National Academy of Sciences* **105**, 2783-2787, doi:10.1073/pnas.0711990105 (2008).

10 Hau, S. K. *et al.* Air-stable inverted flexible polymer solar cells using zinc oxide nanoparticles as an electron selective layer. *Applied Physics Letters* **92**, -, doi:doi:http://dx.doi.org/10.1063/1.2945281 (2008).

Chapter 4

Electric field assisted solvent drying in PBDTTT-C-T: PC70BM solar cells

4.1 PBDTTT-C-T: $PC_{70}BM$ BHJ blend system

The need for the active material to absorb in the IR region along with the visible region of the solar spectrum for higher efficiency of OSCs was required[1]. BHJ-OSCs with low band-gap donors like PCPDTBT[2], PSBTBT[3] and PCDTBT[4] have significantly increased the efficiencies to as high as 7%. There have been reports for a class of benzo(1,2-b:4,5-b′)dithiophene (BDT) based donors polymers which show significant leap, in power conversion efficiency, than its predecessors. These include PBDTTT[5], PBDTTT-C[6], PBDTTT-CF[7], PBDTTT-E-T[8], PBDTTT-C-T. PBDTTT-C-T[8-10] is a high-efficiency donor, which can give efficiencies as higher than 8% with $PC_{70}BM$ as the acceptor.

4.2 Device fabrication

Solar cells with inverted geometry were made from PBDTTT-C-T: $PC_{70}BM$ for this study. ZnO NP were used as the electron buffer layer along with ITO as the electron collecting electrode. MoO_3 was used as the hole collecting buffer and silver was the hole collecting electrodes. Energy band diagram for each layer has been shown in figure 4.1. Fabrication processes were similar to that used for fabricating P3HT: $PC_{60}BM$ devices.

4.2.1 PBDTTT-C-T: $PC_{70}BM$ solution preparation

The optimum blend ratio for PBDTTT-C-T: $PC_{70}BM$ was observed to be 1:1.5, with 10 mg/ml of polymer and 15 mg/ml of $PC_{70}BM$. The solution was made in 1-2 ortho-dichlorobenzene. The solution was stirred overnight at 60^{o}C. 15 minutes prior to spin coating, 3% by volume 1,8-diiodo-octane (DIO) was added to the solution and stirred. Solution is stirred till it was spin coated.

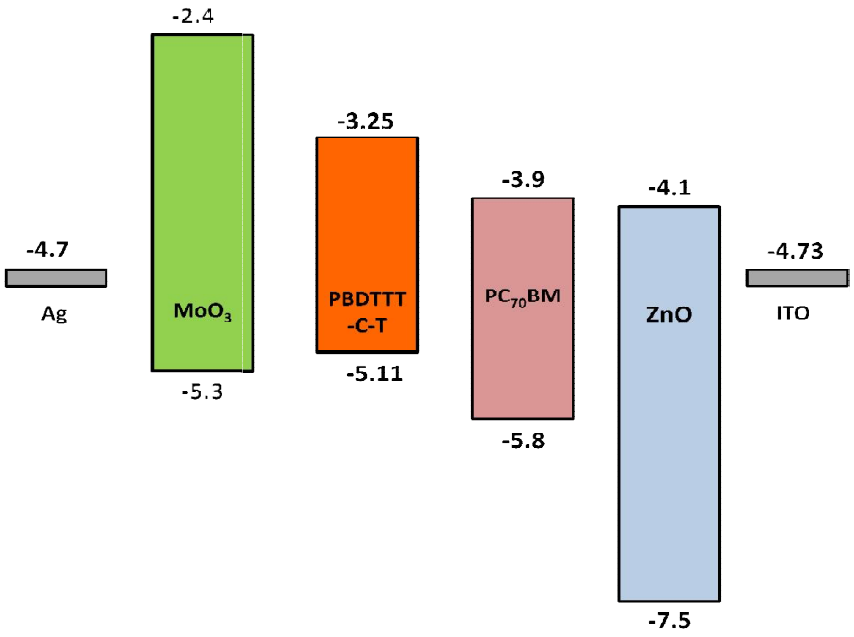

Figure 4. 1: *The band levels of ITO/ZnO/PBDTTT-C-T: $PC_{70}BM$/MoO_3/Ag. The numerical values in the image are electron energy values in eV.*

4.3 Thermal annealing and thermal annealing in electric field

In low band-gap polymer solar cells, thermal annealing has been found to be detrimental to device performance. Similar to the P3HT: $PC_{60}BM$ systems, thermal annealing and thermal annealing in electric field were attempted in PBDTTT-C-T: $PC_{70}BM$ systems. Un-annealed (UA), thermal annealed (TA) and thermal annealed in electric field (TAIE) solar cells were fabricated. The table 4.2.1 summarizes the average (~ 5 devices in each set) and best results obtained in each case.

4.3.1 J-V characteristics of UA, TA and TAIE samples

From the table below, it is clear that thermal annealing is not only ineffective as far as performance parameters are concerned, it sometimes appears detrimental. Thermal annealing in electric field does not have an appreciable effect on the device performance. Considerable drop in FF and J_{sc} reflects as decrease in efficiency. The percentage of devices failures increases on thermal treatments.

		Voc (V)	J_{sc} (mA/cm^2)	Fill Factor	Efficiency (%)
Average	UA	0.76	11.66	48.83	3.93
	TA	0.74	11.6	47.57	3.71
	TAIE	0.74	10.8	48.27	3.53
Best	UA	0.77	12.62	52.84	4.69
	TA	0.74	11.6	47.57	3.71
	TAIE	0.75	11.04	49.46	3.7

Table 4. 1: *Average and best device performance of ITO/ZnO (NP)/PBDTTT-C-T: $PC_{70}BM/MoO_3$/Ag for UA, TA and TAIE samples*

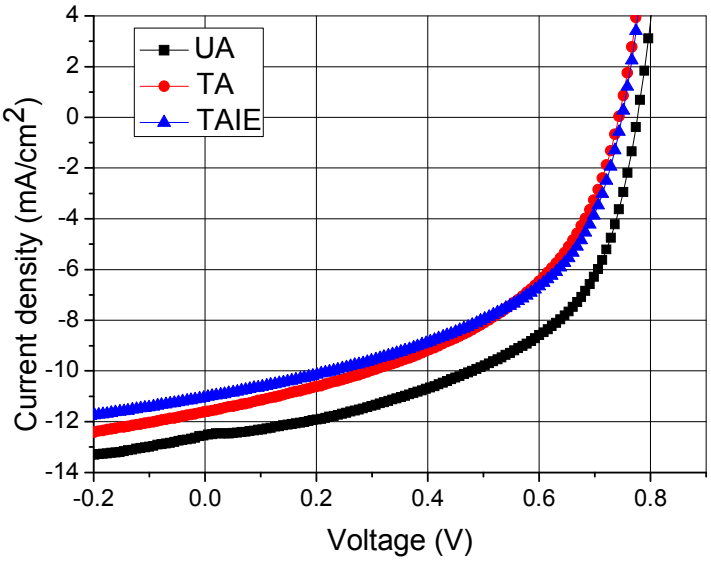

Figure 4. 2: *J-V characteristics for best device performance of ITO/ZnO (NP)/PBDTTT-C-T: $PC_{70}BM/MoO_3$/Ag for UA, TA and TAIE samples.*

4.4 Vacuum treatment and electric field under vacuum

The spin-coated active layer contains DIO as an additive which is a high boiling solvent. Reports suggest vacuum treatment of the spin coated active layer increases device performance, by increasing the rate of removal of solvent from the medium. Vacuum treatment and vacuum treatment under electric field were studied for PBDTTT-C-T: $PC_{70}BM$

solar cells. Along with Un-annealed (UA) solar cells, solar cells were Vacuum treated (VT) as well as vacuum treatment under electric field (VTIE).

4.4.1 Experimental setup

Vacuum treatment

After spin coating the cells were placed in a vacuum chamber outside the glove box. Rotary vane pump was used to create vacuum, cell were kept in a pressure of ~ 10^{-2} mbar for 1 hour. After which the cells were transferred to glove box.

Vacuum treatment in electric field

For VTIE samples, another ITO slide was placed on top of the spin-coated active layer, separated by a spacer. The arrangement was moved to the vacuum chamber. Electrical contacts were taken from each of the ITO slides. The chamber was sealed and vacuum was applied. Electric field was applied, by the voltage source through the external contacts. Electric field and vacuum was applied for 1 hour, after which the samples were moved to the vacuum chamber.

4.4.2 J-V characteristics of UA, VT and VTIE samples

The average (~ 5 devices in each set) and best results of J-V characterization is summarized in the table 4.2. The J_{sc} of the VTIE shows noticeable increase when compared to vacuum treated and un-annealed samples. This observation can be attributed to the formation of better morphology in active layer. It is observed that vacuum treatment without applying electric field has performance similar to UA cells.

It can be seen in table 4.2 that the Voc remains constant irrespective to any treatments performed on the cells. For VTIE samples, the relative percentage increase in J_{sc} and η values are 22.53% and 15.52% respectively, when compared with UA samples, on average.

		Voc (V)	J_{sc} (mA/cm^2)	Fill Factor	Efficiency (%)
Average	UA	0.76	11.66	48.83	3.93
	VT	0.75	11.81	47.9	3.88
	VTIE	0.75	14.17	47.02	4.54
Best	UA	0.77	12.62	52.84	4.69
	VT	0.77	12.042	49.93	4.23
	VTIE	0.77	13.79	49.7	4.8

Table 4. 2: *Average and best device performance of ITO/ZnO (NP)/PBDTTT-C-T: $PC_{70}BM/MoO_3$/Ag for UA, VT and VTIE samples.*

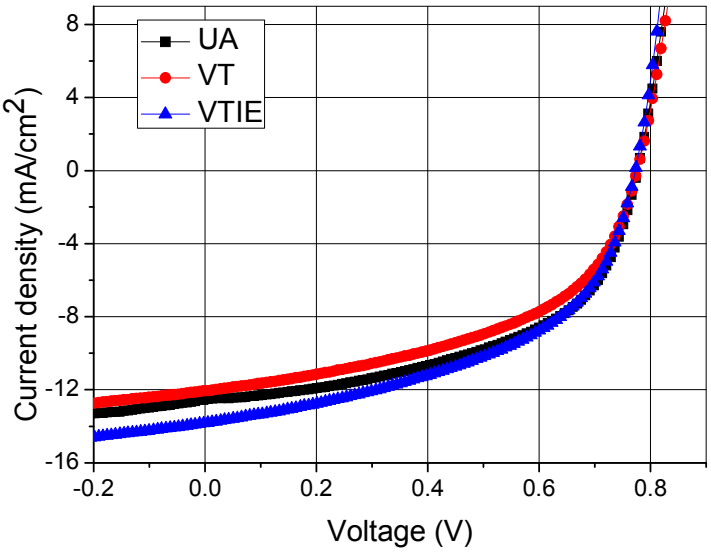

Figure 4. 3: *J-V characteristics for best device performance of ITO/ZnO (NP)/PBDTTT-C-T: $PC_{70}BM/MoO_3$/Ag for UA, VT and VTIE samples*

4.4.3 IPCE spectrum

Figure 4.4 shows IPCE spectrum for UA, VT and VTIE cells, VTIE shows significant increase in IPCE over the entire spectrum. This suggests that the film morphology has been modified by electric field to favour better charge transport. $IPCE_{max}$ for VTIE is 53% (654 nm). The IPCE of UA and VT samples overlap with each other indicating similar morphologies. $IPCE_{max}$ for UA and VT is 46% (656 nm) and 47% (658 nm).

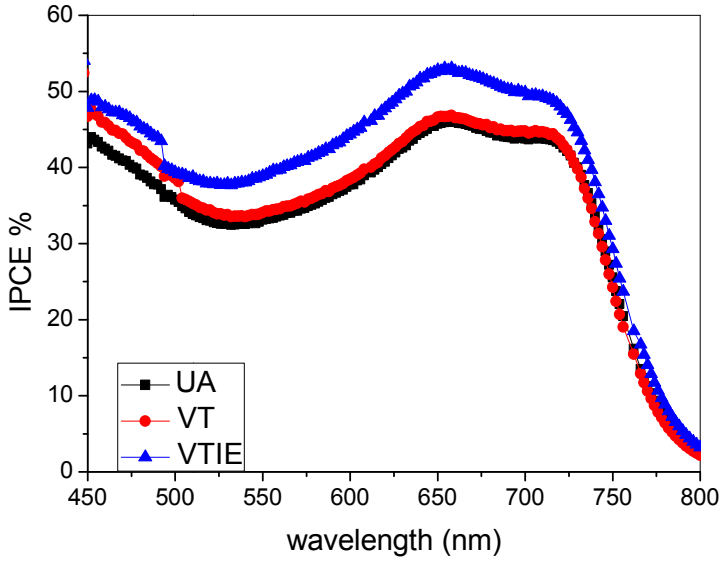

Figure 4. 4: *IPCE spectrum of ITO/ZnO (NP)/PBDTTT-C-T: $PC_{70}BM/MoO_3$/Ag for UA, VT and VTIE samples*

4.5 Discussion

The morphological changes in the film can be explained using figure 4.5,

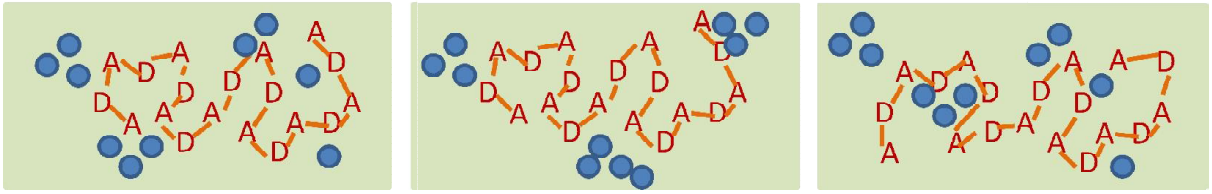

(a) UA/VT *(b) TA/TAIE* *(c) VTIE*

Figure 4. 5: *Schematic representation of morphological changes induced when the samples are unannealed, vacuum treated (a); thermally annealed, thermally annealed in electric field (b); vacuum treatment in electric field (c)*

It should be noted that all samples including UA samples, undergo vacuum treatment before thermal deposition, since thermal deposition is done at very high vacuum conditions. VT samples and UA samples have similar morphology, which reflects in the similar device characteristics for UA and VT cells. It is expected that PBDTTT-C-T polymer chains form dense phases and $PC_{70}BM$ domains are of optimum domain sizes required for efficient charge transport.

Reports have claimed that thermal annealing is detrimental to device performance for the solar cells. Since diffusion of PCBM increases at high temperatures, we speculate that thermal annealing increases $PC_{70}BM$ diffusion making larger domains of PCBM, which are not favourable for efficient charge transport. Thermal annealing in electric field does not create a significant difference as the role played by entropy is higher than the role played by electric field in deciding the morphology of the film.

For the VT and VTIE cases, increasing the rate of evaporation of solvent favours formation of better morphology. Since low band-gap polymers like PBDTTT-C-T have alternating donor and acceptor species, its local dipole moment is expected to be higher. Applying electric field realigns the polymer forming less-dense and more porous domains as indicated by the figure 4.5c. This leads to increased interface with PCBM domains, which ultimately reflects in higher J_{sc} values.

4.5.1 Latest batch

For the latest batch of devices, ZnO NP solution concentration was reduced to half and the solution was spin-coated at 2000 rpm for 30 minutes. This modified process resulted in reducing the thickness of the ZnO buffer layer. Devices were fabricated with all other parameters remaining the same. This new batch of devices showed higher J_{sc} and efficiency values. The samples made were all un-annealed.

	Voc (V)	J_{sc} (mA/cm^2)	Fill Factor	Efficiency (%)
Average	0.78	14.02	56.29	5.57
Best	0.78	14.51	55.74	5.7

Table 4. 3: *Average and best device performance of ITO/ZnO (NP)/PBDTTT-C-T: $PC_{70}BM/MoO_3$/Ag cells of the latest batch where ZnO thickness was varied (only UA samples)*

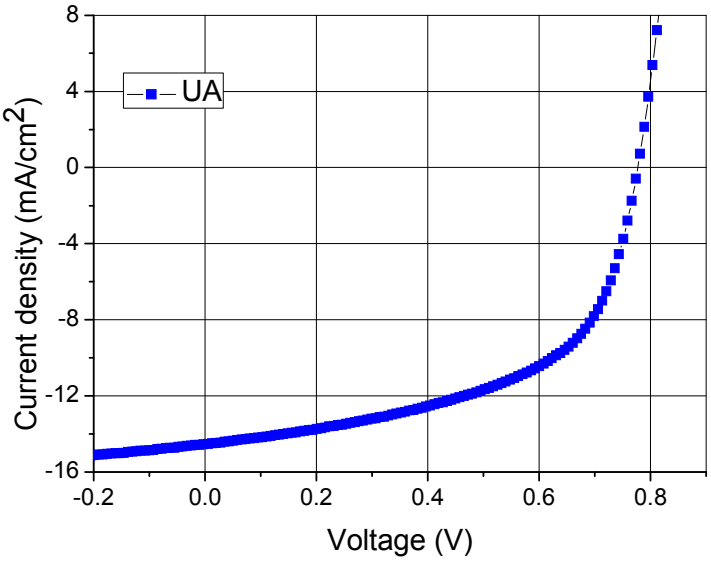

Figure 4. 6: *J-V characteristics of best device of ITO/ZnO (NP)/PBDTTT-C-T: $PC_{70}BM/MoO_3/Ag$ (UA sample)*

4.6 Conclusion and future directions

Applying electric field during vacuum treatment has been found to be beneficial for the device performance in PBDTTT-C-T: PC_{70} BM systems. The exact mechanism, by which electric field during vacuum treatment helps in forming better optimized morphology, is yet to be understood.

As far as we know, this is the first work where applying electric field during vacuum treatment has been used to optimize film morphology in organic solar cells. This treatment opens up a new way where thermodynamics and kinetics of morphological changes could be studied and controlled. This is especially beneficial for low band-gap amorphous donors, where thermal annealing has been found not to be effective.

Correlation of the device performance with AFM studies for each of the case would provide us with a better picture of the morphological changes introduced. It is also expected that vacuum treatment under electric field should provide better performance than un-annealed samples in the recent optimized devices as well.

4.7 References

1 Kroon, R., Lenes, M., Hummelen, J. C., Blom, P. W. M. & de Boer, B. Small Bandgap Polymers for Organic Solar Cells (Polymer Material Development in the Last 5 Years). *Polymer Reviews* **48**, 531-582, doi:10.1080/15583720802231833 (2008).

2 Peet, J. *et al.* Efficiency enhancement in low-bandgap polymer solar cells by processing with alkane dithiols. *Nat Mater* **6**, 497-500, doi:http://www.nature.com/nmat/journal/v6/n7/suppinfo/nmat1928_S1.html (2007).

3 Hou, J., Chen, H.-Y., Zhang, S., Li, G. & Yang, Y. Synthesis, Characterization, and Photovoltaic Properties of a Low Band Gap Polymer Based on Silole-Containing Polythiophenes and 2,1,3-Benzothiadiazole. *Journal of the American Chemical Society* **130**, 16144-16145, doi:10.1021/ja806687u (2008).

4 Blouin, N. *et al.* Toward a Rational Design of Poly(2,7-Carbazole) Derivatives for Solar Cells. *Journal of the American Chemical Society* **130**, 732-742, doi:10.1021/ja0771989 (2007).

5 Liang, Y. *et al.* Development of New Semiconducting Polymers for High Performance Solar Cells. *Journal of the American Chemical Society* **131**, 56-57, doi:10.1021/ja808373p (2008).

6 Hou, J. *et al.* Synthesis of a Low Band Gap Polymer and Its Application in Highly Efficient Polymer Solar Cells. *Journal of the American Chemical Society* **131**, 15586-15587, doi:10.1021/ja9064975 (2009).

7 Chen, H.-Y. *et al.* Polymer solar cells with enhanced open-circuit voltage and efficiency. *Nat Photon* **3**, 649-653 (2009).

8 Huo, L. *et al.* Replacing Alkoxy Groups with Alkylthienyl Groups: A Feasible Approach To Improve the Properties of Photovoltaic Polymers. *Angewandte Chemie International Edition* **50**, 9697-9702, doi:10.1002/anie.201103313 (2011).

9 Adhikary, P. *et al.* Enhanced charge transport and photovoltaic performance of PBDTTT-C-T/PC70BM solar cells via UV-ozone treatment. *Nanoscale* **5**, 10007-10013, doi:10.1039/c3nr03355d (2013).

10 Li, X. *et al.* Dual Plasmonic Nanostructures for High Performance Inverted Organic Solar Cells. *Advanced Materials* **24**, 3046-3052, doi:10.1002/adma.201200120 (2012).